

RL-TR-91-43  
In-House Report  
April 1991

AD-A255 189



2

# PRACTICAL CONSIDERATIONS RELATIVE TO THE DESIGN AND MANUFACTURE OF MICROSTRIP ANTENNAS

Daniel A. Mullinix, Capt, USAF

SEP 10 1992

*APPROVED FOR PUBLIC RELEASE; DISTRIBUTION UNLIMITED.*

Rome Laboratory  
Air Force Systems Command  
Griffiss Air Force Base, NY 13441-5700

92 9 23 008

92-25691



This report has been reviewed by the Rome Laboratory Public Affairs Division (PA) and is releasable to the National Technical Information Service (NTIS). At NTIS it will be releasable to the general public, including foreign nations.

RL-TR-91-43 has been reviewed and is approved for publication.

APPROVED:



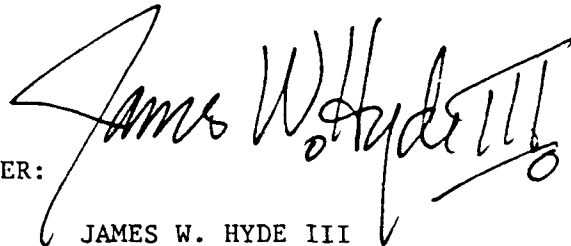
ROBERT J. MAILLOUX  
Chief, Antennas & Components Division  
Directorate of Electromagnetics

APPROVED:



JOHN K. SCHINDLER  
Director of Electromagnetics

FOR THE COMMANDER:



JAMES W. HYDE III  
Directorate of Plans & Programs

If your address has changed or if you wish to be removed from the Rome Laboratory mailing list, or if the addressee is no longer employed by your organization, please notify Rome Laboratory (EEA) Hanscom AFB MA 01731-5000. This will assist us in maintaining a current mailing list.

Do not return copies of this report unless contractual obligations or notices on a specific document require that it be returned.

REPORT DOCUMENTATION PAGE			Form Approved OMB No. 0704-0188	
Public reporting for this collection of information is estimated to average 1 hour per response, including the time for reviewing instructions, searching existing data sources, gathering and maintaining the data needed, and completing and reviewing the collection of information. Send comments regarding this burden estimate or any other aspect of this collection of information, including suggestions for reducing this burden, to Washington Headquarters Services, Directorate for Information Operations and Reports, 1215 Jefferson Davis Highway, Suite 1204, Arlington, VA 22202-4302, and to the Office of Management and Budget, Paperwork Reduction Project (0704-0188), Washington, DC 20503.				
1. AGENCY USE ONLY (Leave blank)		2. REPORT DATE April 1991		3. REPORT TYPE AND DATES COVERED In-House Report Jan 89 - Apr 90
4. TITLE AND SUBTITLE Practical Considerations Relative to the Design and Manufacture of Microstrip Antennas			5. FUNDING NUMBERS PE 62702F PE 61102F PR 4600 PR 2305 TA 14 TA J3 WU 01 WU 03	
6. AUTHOR(S) Daniel A. Mullinix, Capt, USAF				
7. PERFORMING ORGANIZATION NAME(S) AND ADDRESS(ES) Rome Laboratory (EEA) Hanscom AFB, MA 01731-5000			8. PERFORMING ORGANIZATION REPORT NUMBER RL-TR-91-43	
9. SPONSORING/MONITORING AGENCY NAME(S) AND ADDRESS(ES)			10. SPONSORING/MONITORING AGENCY REPORT NUMBER	
11. SUPPLEMENTARY NOTES				
12a. DISTRIBUTION/AVAILABILITY STATEMENT Approved for Public Release: Distribution Unlimited			12b. DISTRIBUTION CODE	
13. ABSTRACT (Maximum 200 words) Practical considerations relative to the design and manufacture of microstrip antennas are poorly documented. This report contains practical information on models, substrates, connectors, manufacturing error and feed designs as they relate to microstrip antennas. Two new versions of the transmission line model are introduced and compared to the original version and the model expansion cavity model. Three sets of rectangular patch antennas were constructed on $\epsilon_r = 2.52$ , 4.4, and 6.0 substrates, respectively, and measured. All models were programmed and compared to these measured results. One new transmission line model achieved less than 0.7 percent resonant frequency error compared to 3 percent error for the original model on the $\epsilon_r = 2.52$ substrate. The cavity model also performed well with 1.2 percent and 0.64 percent error for the $\epsilon_r = 2.52$ and $\epsilon = 6.0$ substrates, respectively. The $\epsilon_r = 4.4$ epoxy substrate was deemed unacceptable due to high losses and a poor $\epsilon_r$ tolerance.				
14. SUBJECT TERMS Microstrip Antennas Conformal Antennas Microstrip Components Printed Circuit Antennas			15. NUMBER OF PAGES 36	
			16. PRICE CODE	
17. SECURITY CLASSIFICATION OF REPORT Unclassified	18. SECURITY CLASSIFICATION OF THIS PAGE Unclassified	19. SECURITY CLASSIFICATION OF ABSTRACT Unclassified	20. LIMITATION OF ABSTRACT SAR	

A-1

100% QUALITY INSPECTED 3

## Contents

1. INTRODUCTION	1
2. THEORY	3
2.1 Edge Fed Rectangular Patch Using Transmission Line Model	3
2.2 Stagger Tuned Patch Using Transmission Line Model	11
2.3 Rectangular Patch Using Modal Expansion Cavity Model	13
3. PRACTICAL DESIGN AND MANUFACTURING CONSIDERATIONS AND CONSTRAINTS	19
3.1 Introduction	19
3.2 Connectors	19
3.3 Substrate Selection and Manufacturing Errors	21
3.4 Feed Design (Transformer vs Inset vs Probe vs Offset)	29
3.5 Model and Physical Limitations	31
4. EXPERIMENTAL RESULTS AND DISCUSSION	33
4.1 Introduction	33
4.2 Manufacturing Error	37
4.3 Rectangular Patch Measurement Results	39
4.4 Stagger Tuned Patch Measurement Results	44
5. CONCLUSIONS AND RECOMMENDATIONS	45
REFERENCES	47
APPENDIX A: Rectangular Patch Measurements	49
APPENDIX B: Stagger Tuned Patch Measurements	69

## Illustrations

1. Microstripline Fed Rectangular Patch	4
2. Rectangular Patch Radiating Slots and Equivalent Circuit	4
3. Stagger Tuned Patch	12
4. Stagger Tuned Patch Radiating Slots and Equivalent Circuit	12
5. Probe Feed and Offset Feed Rectangular Patches	14
6. Common Microstrip Connectors	21
7. Microstrip Patch Size Comparison vs Frequency for $\epsilon_r = 2.52, 4.4$ and $6.0$	22
8. Microstripline Width vs Impedance	23
9. Rectangular Patch Center Edge Impedance vs Frequency for $\epsilon_r = 2.52, 4.4$ and $6.0$	24
10. Theoretical 2:1 VSWR Bandwidth vs Frequency	27
11. Rectangular Microstrip Patch Efficiency	29
12. Inset Feed Rectangular Patch	31
13a. Rectangular Patch on $\epsilon_r = 2.52$	34
13b. Rectangular Patch on $\epsilon_r = 4.4$	35
13c. Rectangular Patch on $\epsilon_r = 6.0$	36
13d. Stagger Tuned Patch on $\epsilon_r = 2.52$	37

14. Manufacturing Error vs Frequency	38
15. Model Error vs Resonant Frequency $\epsilon_r = 2.52$	40
16. Model Error vs Resonant Frequency $\epsilon_r = 6.0$	41
17. Model Error vs Resonant Frequency $\epsilon_r = 4.4$	42
18. Measured 2:1 VSWR Bandwidth vs Resonant Frequency	44
19. Stagger Tuned Patch Model Error vs Resonant Frequency	45

## Tables

1. Commercial Substrate Tolerances	25
2. Surface Wave Mode Cutoff Frequencies	31
3. Manufacturing Error	39
4. Rectangular Patch Input Impedances	43

## **Preface**

I thank the USAF Rome Laboratory (RL) (formerly Rome Air Development Center (RADC)) Electromagnetics Directorate for co-sponsoring this report. I would also like to thank Mr. James Kenny and Mr. Erhard Wisniewski of the RL Electromagnetics Measurement Facility for their help in measuring and manufacturing the patch antennas.

# **Practical Considerations Relative to the Design and Manufacture of Microstrip Antennas**

## **1. INTRODUCTION**

Many variables exist in the design and manufacture of printed circuit antennas. Models range from simple transmission line models which are relatively easy to understand and program to full-wave methods which are much more difficult to understand and may take weeks or even months to develop and program. One of the biggest problems associated with most models is that there are many different equations in the literature for computing the effective dielectric constant, the radiation admittance at the patch edges and the fringing field length extensions. Model accuracy varies considerably depending on the equations used. Substrate materials range from the PTFE (Polytetrafluoroethylene) with a dielectric constant of 2.2-2.5, to GaAs with a dielectric constant of 12.9. Some of these materials consistently produce good antennas and some are very troublesome to work with and can require several iterations to obtain the desired resonant frequency and input impedance due to  $\epsilon_r$  tolerances, manufacturing tolerances and model limitations. Microwave connectors range from SMA (Sub-Miniature Adapter) probes and tabs to Wiltron V-Series connectors. Available connector dimensions can restrict the designer to a small range of substrate thicknesses and can influence the patch feed design. Feed types include probe feeds, inset feeds, transformer edge feeds and offset edge feeds. The type of feed normally depends on the application. Each of

---

(Received for publication 25 March 1991)



these feeds has restrictions that must be considered or shifts in the resonant frequency and poor matching can occur. Other anomalies, like surface waves and dispersion, can result from increasing the frequency or the electrical thickness of the substrate. Surface waves can cause reduced efficiency in single elements and scan blindness in arrays. Dispersion causes the dielectric constant to become a function of frequency. Knowledge of these details is essential to the success of the microstrip antenna designer.

This report is written from the viewpoint of an antenna designer gazing upon the vast myriad of papers and books on this topic. All of the popular patch antenna models can design patches to within a "few percent" of the desired resonant frequency; however, since most of these antennas are narrow band, more than a "few percent" accuracy is needed if we want a CAD designed antenna to be resonant in-band on the first iteration.

In the transmission line model, a rectangular patch is modelled as two narrow H-plane radiating slots separated from the feed by a section of microstripline whose width is equal to the patch width  $a$ . The admittance of these slots is transformed through the microstripline to the feedpoint giving an input admittance. In Munson's<sup>1</sup> transmission line model, fringing fields are accounted for by a length reduction factor  $q$  which is empirically determined, and the patch admittance is computed using an equation that neglects the effective dielectric constant and the conductor thickness. Better accuracy can be obtained by using the effective dielectric constant, more accurate patch and slot admittance equations, and by adding a published equation for the fringing field length extension of an open circuited microstripline to the electrical length of the patch.

In modal expansion cavity models,<sup>2</sup> the region between the microstrip patch and the ground plane is treated as a cavity bounded by magnetic walls along the edges and by electric walls from above and below. The loss due to radiation is represented by an impedance boundary condition at the walls.

For this report, I propose to identify and discuss practical considerations needed by the working engineer tasked with designing microstrip antennas. First, I will investigate models, and compare different approaches and equations for the effective dielectric constant, radiation admittance at the patch edge and length extensions for the transmission line model. These will be compared to the original transmission line model, the modal expansion cavity model, and measured results. The effects of manufacturing errors will also be discussed. Three sets of transformer edge fed rectangular patches were constructed and measured as part of this report on  $\epsilon_r = 2.52$ , 4.4, and 6.0. Each set was constructed on a different  $\epsilon_r$  substrate and consists of seven patches with resonant frequencies between 4 and 16 GHz. A set of stagger-tuned patches was also constructed on  $\epsilon_r = 2.52$  substrate material. I will also discuss practical design and manufacturing considerations with regard to connectors, substrates, manufacturing errors, feed designs, and model and physical limitations. Many figures and graphs are included in this section to give the reader a database they can use for future reference for their own

---

<sup>1</sup> Munson, R.E. (1974) Conformal microstrip antennas and microstrip phased arrays, *IEEE Trans. Antennas and Propagation*, **AP-22**:74-78.

<sup>2</sup> Carver, K.R. and Mink, J.W. (1981) Microstrip antenna technology, *IEEE Trans. Antennas and Propagation*, **AP-29**:25-37.

designs. Unfortunately, the computer programs written for the models could not be included in this report due to the software public release regulations of the Rome Laboratory. However, I have included detailed design instructions that reference equation numbers for both the transmission line and cavity models to facilitate easier programming.

## 2. THEORY

### 2.1 Edge Fed Rectangular Patch Using Transmission Line Model

An edge-fed rectangular patch is shown in Figure 1. The length and width are labeled  $a$  and  $b$  as is customary and the patch is fed using a combination of two  $\lambda_g/4$  impedance transformers and an  $n\lambda_g/2$  section of microstripline as shown in Figure 1. In the transmission line model, a rectangular patch is modelled as two radiating slots separated by a section of microstripline. The slots are located on the edges of the patch perpendicular to the feedline as shown in Figure 2. The radiation from these slots is represented by equivalent slot admittances as schematically shown in the equivalent circuit of Figure 2. Expressions for the characteristic admittance and effective dielectric constant of the microstripline patch segment, which take into account the effects of strip thickness, are given by *Bahl and Garg*<sup>3</sup> as:

$$Y_C = \frac{\sqrt{\epsilon_{re}}}{\eta_0} \left[ \frac{a_e}{h} + 1.393 + .667 \ln \left( \frac{a_e}{h} + 1.444 \right) \right], \quad (1a)$$

where  $\eta_0 = (\mu_0/\epsilon_0)^{1/2}$ ,

$$a_e = a + \frac{1.25t}{\pi} \left[ 1 + \ln \left( \frac{2h}{t} \right) \right], \quad a \geq \frac{h}{2\pi}, \quad (1b)$$

and

$$\epsilon_{re} = \frac{\epsilon_r + 1}{2} + \frac{\epsilon_r - 1}{2\sqrt{1+10\frac{h}{a}}} - \frac{\epsilon_r - 1}{4.6} \frac{\frac{t}{h}}{\sqrt{\frac{a}{h}}}. \quad (1c)$$

<sup>3</sup> Bahl, I.J. and Garg, Ramesh (1977) Simple and accurate formulas for microstrip with finite strip thickness, *Proc. IEEE*, **65**:1611-1612.

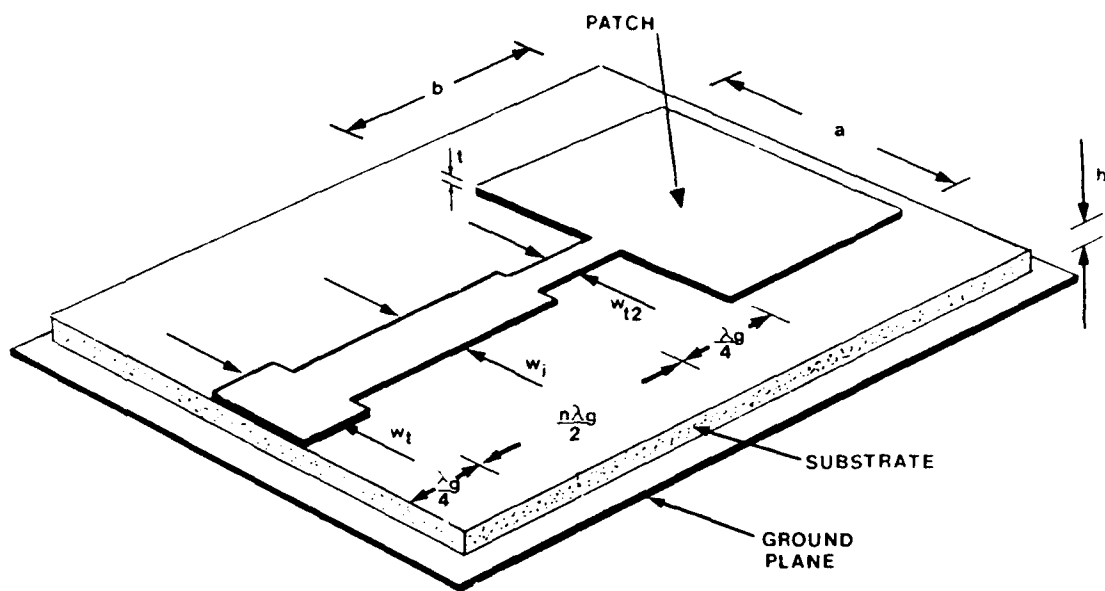


Figure 1. Microstripline Fed Rectangular Patch

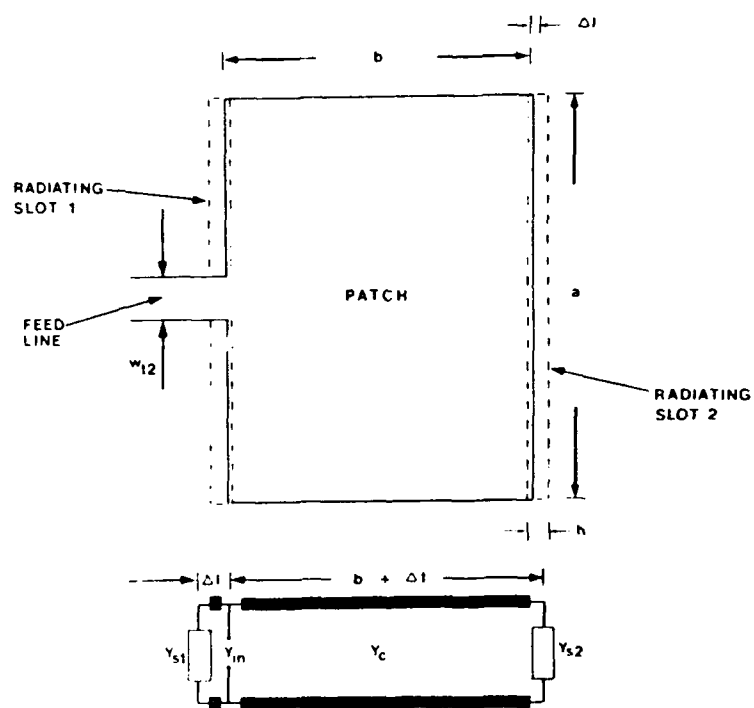


Figure 2. Rectangular Patch Radiating Slots and Equivalent Circuit

The effective dielectric constant,  $\epsilon_{re}$ , is also given by *Schneider*<sup>4</sup> and *Hammerstadt*<sup>5</sup> as:

$$\epsilon_{re} = \frac{\epsilon_r + 1}{2} + \frac{\epsilon_r - 1}{2} \left( 1 + 12 \frac{h}{a_e} \right)^{-1/2}, \quad \frac{a}{h} \geq 1, \quad (2a)$$

with

$$a_e = a + \frac{t}{\pi} \left( 1 + \ln \left( \frac{2h}{t} \right) \right), \quad \frac{a}{h} \geq \frac{1}{2\pi}. \quad (2c)$$

Finally, *Hammerstadt and Jenson*<sup>6</sup> give the following equations for the patch characteristic admittance  $Y_C = 1/Z_C$  and the effective dielectric constant  $\epsilon_{re}$  as:

$$Z_C = \frac{1}{\sqrt{\epsilon_{re}}} \frac{\eta_0}{2\pi} \ln \left[ \frac{F_1 h}{a} + \left( 1 + \left( \frac{2h}{a} \right)^2 \right)^{1/2} \right], \quad (3a)$$

where

$$F_1 = 6 + (2\pi - 6) \exp \left( - \left( 30.666 \frac{h}{a} \right)^{0.7528} \right), \quad (3b)$$

and

$$\epsilon_{re} = \frac{\epsilon_r + 1}{2} + \frac{\epsilon_r - 1}{2} \left( 1 + \frac{10h}{a} \right) - (A)(F), \quad (3c)$$

<sup>4</sup> Schneider, M.V. (1969) Microstrip Lines for Microwave Integrated Circuits, *Bell System Technical Journal*, pp. 1421-1444.

<sup>5</sup> Hammerstadt, E.O. (1975) Equations for microstrip circuit design, *Proc. European Microwave Conference*, Hamburg, Germany, Sept. 1975, pp. 268-272.

<sup>6</sup> Hammerstadt, E.O. and Jenson, O. (1980) Accurate models for microstrip computer aided design, *IEEE MTT-S Int. Microwave Symposium Digest*, pp. 407-409.

with

$$A = 1 + \frac{1}{49} \ln \left[ \frac{(a/h)^4 + [a/(52h)]^2}{(a/h)^4 + 0.432} \right] + \frac{1}{18.7} \ln \left[ 1 + \left( \frac{a}{18.1h} \right)^3 \right] \quad (3d)$$

and

$$B = 0.564 \left[ \frac{\epsilon_r - 0.9}{\epsilon_r + 3} \right]^{0.053} \quad (3e)$$

Several equations have similarly been published<sup>7,8,9</sup> in the literature for computing the slot admittance  $Y_S$ . Munson's paper<sup>1</sup> uses equations by Harrington<sup>7</sup> for the admittance of a *TE* excited waveguide radiating into a half-space as the microstrip patch slot admittance equations. The equation used for the slot admittance  $Y_S$  is given as<sup>7</sup>.

$$Y_S = \frac{\pi a}{\lambda_o \eta_o} \left[ 1 - \frac{(kh)^2}{24} \right] + j \frac{a}{\lambda_o \eta_o} [3.135 - 2 \ln(kh)] , \quad \frac{h}{\lambda_o} \leq .1 \quad (4a)$$

Another equation for computing  $Y_S$  is given in a recent paper by Pues and Van de Capelle<sup>8</sup> as:

$$Y_S = G_S + jB_S \quad (5a)$$

<sup>7</sup> Harrington, R. (1961) *Time Harmonic Electromagnetic Fields*, McGraw-Hill, New York.

<sup>8</sup> Pues, H. and Van de Capelle, A. (1984) Accurate transmission line model for the rectangular microstrip antenna, *IEEE Proc.*, **131**(Pt. H.):334-340.

<sup>9</sup> Gogoi, A. and Gupta, K.C. (1982) Weiner-Hopf computation of edge admittances for microstrip patch radiators, *AEU*, **36**:464-467.

where

$$G_S = \frac{1}{\pi^2 \eta_0} \int_0^\pi \int_0^\pi \frac{\sin^2 \left( \frac{k a_e}{2} \cos \alpha \right) \sin^2 \left( \frac{S}{2} \sin \alpha \cos \beta \right) \sin^3 \alpha}{\cos^2 \alpha \left( \frac{S}{2} \sin \alpha \cos \beta \right)^3} d\alpha d\beta, \quad (5b)$$

and

$$s = k \Delta l \quad (5c)$$

$$\beta = k \sqrt{\epsilon_{re}} \quad (5d)$$

$$\alpha = 0.5 \beta \tan \delta_e. \quad (5e)$$

Tan  $\delta_e$  is the effective loss tangent and  $a_e$  is given by Eq. (1b) or (2c). A Maclaurin series expansion about  $s = 0$  in the normalized slot width  $s$  has been derived for the above integral<sup>8</sup>. Retaining the first two terms results in:

$$G_S = \frac{1}{\pi \eta_0} \left\{ \left( k a_e \operatorname{Si}(k a_e) + \frac{\sin k a_e}{k a_e} + \cos k a_e - 2 \right) \left( 1 - \frac{S^2}{24} \right) - \frac{S^2}{12} \left( \frac{1}{3} + \frac{\cos k a_e}{(k a_e)^2} - \frac{\sin k a_e}{(k a_e)^3} \right) \right\}. \quad (6a)$$

The imaginary part is given as<sup>8</sup>:

$$B_S = Y_C \tan(\beta \Delta l). \quad (6b)$$

In the above equations,  $k = 2\pi/\lambda_0$  and  $\operatorname{Si}()$  is the sine integral. In Eq. (4a), the width of the patch input transformer  $w_{12}$  is subtracted from  $a$  to account for the reduction in the length of the first slot due to the feed line. Also, in this equation,  $\lambda_0$  is the free space wavelength.

In Eqs. (5) and (6), modeling of the parasitic effect of the feedline is accounted for by reducing the admittance of the first slot by a factor  $r$  given by<sup>8</sup>:

$$r = 1 - \frac{W}{a_e} \epsilon_r. \quad (7a)$$

This reduction is incorporated into the model by the addition of a parallel admittance  $Y_F$  at the location of slot 1 in the equivalent circuit of Figure 2.  $Y_F$  is given by<sup>8</sup>:

$$Y_F = (r - 1)Y_s. \quad (7b)$$

The  $\Delta l$  term in the above equations is the fringing field length extension. Fringing fields make the electrical length of a patch slightly longer than its physical length, thus resulting in a patch which resonates at a slightly lower frequency than its physical length would suggest. The classical equation referenced by most papers for the fringing field length extension is given by *Hammerstadt* as<sup>5</sup>:

$$\Delta l/h = 0.412 \frac{[\epsilon_{re} + 0.3][(a/h) + 0.262]}{[\epsilon_{re} - 0.258][(a/h) + 0.813]}. \quad (8a)$$

This equation is a functional approximation of the numerical static results from *Silvester and Benedek*<sup>10</sup> for  $\epsilon_r = 1, 2.5, 4.2, 9.6, 16$  and  $51$  with  $t = 0$ . *Hoffman*<sup>11</sup> gives the accuracy of this equation for  $0.3 \leq a/h \leq 2$  and  $1 \leq \epsilon_r \leq 50$  as 5 percent. *Kirschning, Jansen and Koster*<sup>12</sup> recently published a length extension that is a functional approximation of low frequency calculations from a rigorous hybrid-wave analysis. This length extension is claimed to have accuracy of better than 2.5 percent for  $0.01 \leq a/h \leq 100$  and  $1 \leq \epsilon_r \leq 50$ , and is given as:

$$\Delta l/h = (A) (C) (E/D). \quad (9a)$$

<sup>10</sup> Silvester, P. and Benedek, P. (1972) Equivalent capacitances of microstrip open circuits, *IEEE Trans. On Microwave Theory and Techniques*, Vol. **MTT-20** (No. 8):511-516.

<sup>11</sup> Hoffman, R.K. (1987) *Handbook of Microwave Integrated Circuits*, Artech House.

<sup>12</sup> Kirschning, M., Jansen, R.H., and Koster, N.H.L. (1981) Accurate model for open end effect of microstrip lines, *Electronics Letters*, **17** (No. 3):123-124.

where

$$A = 0.434907 \frac{\left[ \epsilon_{re}^{0.81} + 0.26 \right] \left[ (a/h)^{0.8544} + 0.236 \right]}{\left[ \epsilon_{re}^{0.81} - 0.189 \right] \left[ (a/h)^{0.8544} + 0.87 \right]}, \quad (9b)$$

$$B = 1 + \frac{(a/h)^{0.371}}{2.358\epsilon_r + 1}, \quad (9c)$$

$$C = 1 + \left( \frac{0.5274}{\epsilon_r^{0.9236}} \right) \arctan \left( 0.084 (a/h)^{1.9413/B} \right), \quad (9d)$$

$$D = 1 + 0.0377 \left\{ 6 - 5 \exp[0.036 (1 - \epsilon_r)] \right\} + \arctan \left( 0.067 (a/h)^{1.456} \right), \quad (9e)$$

and

$$E = 1 - 0.218 \exp(-7.5 a/h). \quad (9f)$$

Finally, the length extension given by Gogol and Gupta in their analysis is given as<sup>9</sup>:

$$\Delta l = \frac{0.95h}{1 + 0.85k_0 h} - \frac{0.075h(\epsilon_r - 2.45)}{1 + 10k_0 h} \quad (10a)$$

where the given accuracy range is  $0.1 \leq k_0 h \leq 0.6$  and  $2.45 \leq \epsilon_r \leq 2.65$ .

Once equations are defined for  $Y_C$  and  $Y_S$ , we define  $Y_{S1}$  as the admittance of slot 1 and  $Y_{S2}$  as the admittance of slot 2. Then, using standard transmission line theory, from Figure 2, the input admittance at the feed point is given as:

$$Y_{in} = Y_1 + Y_2, \quad (11a)$$



where  $Y_1$  is given as:

$$Y_1 = \frac{e^{jx_1} - \Gamma_1 e^{-jx_1}}{e^{jx_1} + \Gamma_1 e^{-jx_1}} Y_C, \quad (11b)$$

with

$$x_1 = k\Delta l, \quad (11c)$$

$$\Gamma_1 = \frac{Y_C - Y_{S1}}{Y_C + Y_{S1}}, \quad (11d)$$

and  $Y_2$  is given as:

$$Y_2 = \frac{e^{jx_2} - \Gamma_2 e^{-jx_2}}{e^{jx_2} + \Gamma_2 e^{-jx_2}} Y_C, \quad (11e)$$

$$x_2 = kb \sqrt{\epsilon_{re}} + k\Delta l \quad (11f)$$

with

$$\Gamma_2 = \frac{Y_C - Y_{S2}}{Y_C + Y_{S2}}. \quad (11g)$$

To determine the correct patch dimensions for a given resonant frequency, the following procedure is used:

- (i). Compute an approximate patch length  $b$  for the desired resonant frequency using  $b = 0.49 \lambda_0 / \sqrt{\epsilon_r}$ . Choose a patch width  $a$  between  $b$  and  $2b$  (for example, choosing  $a = 0.65 \lambda_0 / \sqrt{\epsilon_r}$  will give an aspect ratio of  $a/b \approx 1.3$ ).

(ii). Make an initial guess at the real part of the patch edge impedance using Figure 9 and use equations from Gupta<sup>13</sup> to compute the width of the microstrip feedline that corresponds to this value. Compute the admittance of the main patch section which corresponds to its width  $a$  using Eqs. (1a-b) or (3a-b).

(iii). Compute  $\Delta l$  using either Eqs. (8a), ((9a-e), or (10a). Then compute the slot admittances  $Y_{S1}$ ,  $Y_{S2}$  using either Eq. (4a) or (5a-e). If Eq. (4a) is used, then the width of the microstrip feedline must be subtracted from  $a$  for the admittance  $Y_{S1}$  of slot 1. If Eq. (5a-e) or (6a-b) are used, then  $Y_F$  must be computed using Eqs. (7a) and (7b) and added to the admittance  $Y_{S1}$  of slot 1 to account for the partial blockage of slot 1 by the microstrip feedline.

(iv). Equation (11a) is then iterated with successive values of  $b$  until the imaginary part of the input impedance is zero and the microstrip feedline width corresponds to the center edge resistance of the patch.

## 2.2 Stagger Tuned Patch Using Transmission Line Model

A Stagger or "Stub"<sup>14</sup> tuned patch is shown in Figure 3. It was selected for modelling because it is a simple example that demonstrates how transmission line models can be extended to model a variety of patch designs. To use a transmission line model for this patch, we divide the patch into two rectangular segments, a main patch section, and a stub or stagger tuned section. The main patch section is modelled, as is customary, by two radiating slots, while the stagger tuned section adds a third slot. The slots are located on the edges of the patch perpendicular to the feedline as shown in Figure 4. The slots are again represented by equivalent admittances that are transformed through the network of transmission line segments to the feedpoint, giving an input admittance as schematically shown in Figure 4. In this figure,  $l_1$  and  $l_2$  are the lengths, and  $w_1$  and  $w_2$  are the widths of the main and stagger tuned sections respectively. The characteristic admittances of these sections are denoted  $Y_{C1}$  and  $Y_{C2}$  respectively and are computed using Eqs. (1a) or (3a). Similarly, the admittances of slots 1 through 3 are denoted  $Y_{S1}$ ,  $Y_{S2}$  and  $Y_{S3}$ , and are computed using either Eqs. (4a) or (5a).

<sup>13</sup> Gupta, K.C., Garg, R., and Chadha, R. (1981) *Computer Aided Design of Microwave Circuits*, Artech House.

<sup>14</sup> Pozar, D.M. (1987) Trimming stubs for microstrip feed networks and patch antennas. *IEEE Antennas and Propagation Society Newsletter*, Dec. 1987.

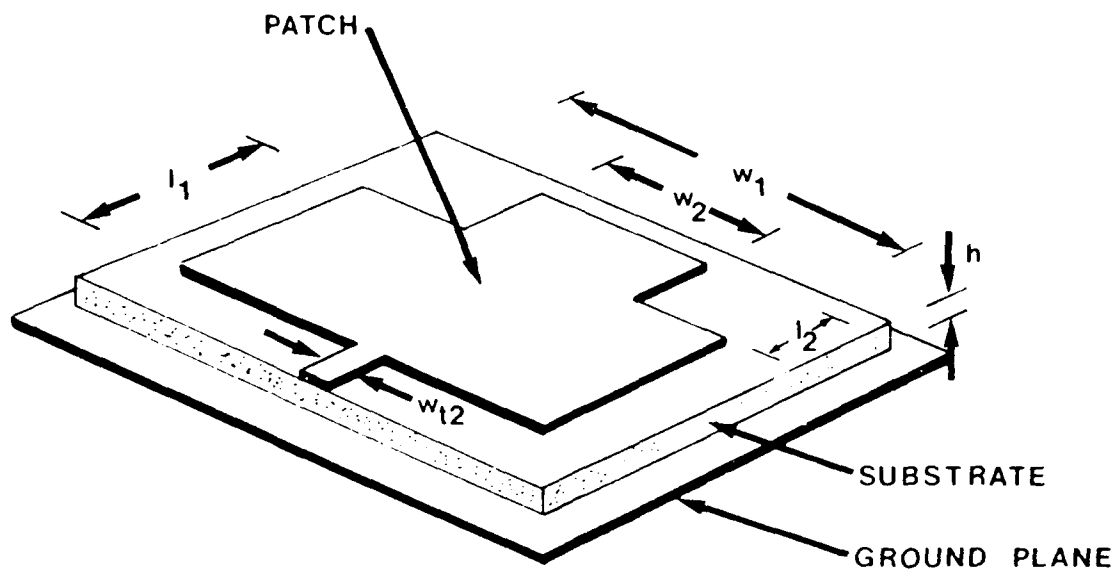


Figure 3. Stagger Tuned Patch

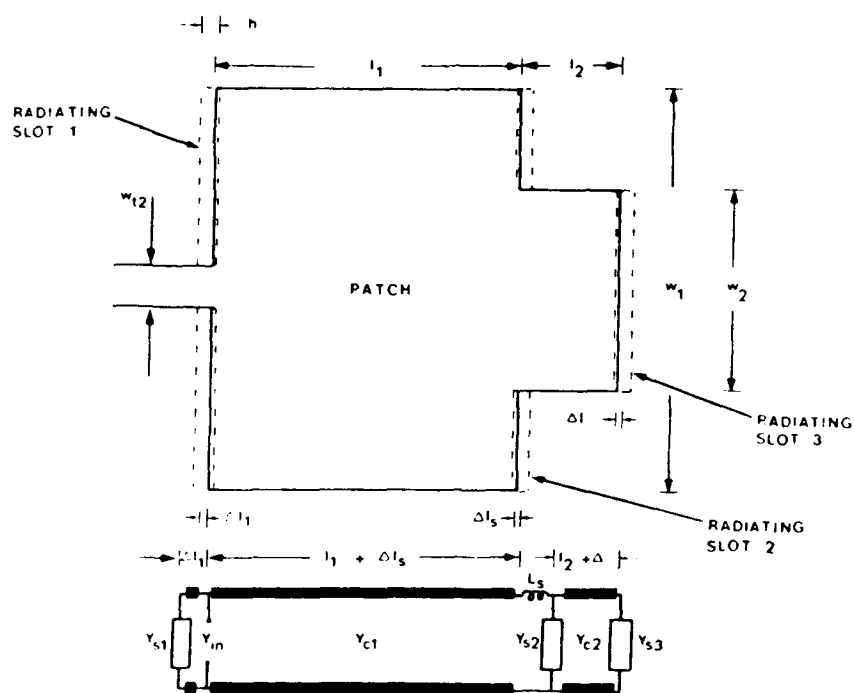


Figure 4. Stagger Tuned Patch Radiating Slots and Equivalent Circuit

The series inductance  $L_S$  in the equivalent circuit of Figure 4 is generated by the increase in current density as one goes from a wider to a narrower microstripline and is given by *Hoffman* as:<sup>11</sup>

$$L_S = \frac{h\mu_0}{\pi} \ln \left\{ \frac{1}{\sin \left( \frac{\pi}{2} \frac{Z_{C1} \sqrt{\epsilon_{re,1}}}{Z_{C2} \sqrt{\epsilon_{re,2}}} \right)} \right\} \quad (12a)$$

where  $Z_{C1}$  and  $Z_{C2}$  are equal to  $1/Y_{C1}$  and  $1/Y_{C2}$  respectively. Also, the fringing fields on the front edge of the wider main patch section generates a shunt capacitance  $C_P$  given as:<sup>11</sup>

$$C_P = \left[ \frac{\sqrt{\epsilon_{re,1}}}{Z_{C1} c_0} - \frac{\epsilon_0 \epsilon_r w_1}{h} \right] \left[ \frac{(w_1 - w_2)}{2} \right] \quad (13a)$$

where  $c_0$  is the speed of light. However, for the usual case where  $w_1$  and  $w_2$  are  $\gg h$ , this series inductance is very small compared to the shunt capacitance and is neglected. The shunt capacitance is represented equivalently as a length extension  $\Delta l_s$  and is given by *Hoffman*<sup>11</sup> as:

$$\Delta l_s = h \left[ \frac{1.35}{\epsilon_r} + 0.44 \right] \left[ 1 - \frac{w_2}{w_1} \right] \quad (14a)$$

The design procedure is the same here as for the rectangular patch in Section 2.1, that is, the total patch length  $l_1 + l_2$  is iterated until the input admittance  $Y_{in}$  is purely real.

### 2.3 Rectangular Patch Using Modal Expansion Cavity Model

The modal expansion cavity model is a slightly more complex yet still easy to implement alternative to the transmission line model. It is also a "better" model since it takes into account the field variations along the radiating edges of the patch which in turn allows you to compute the input impedance at any location on the patch. In contrast, the transmission line model can only accurately predict the input impedance at the center of a radiating edge.

Offset and probe feed versions of a rectangular patch with length  $b$  and width  $a$  are shown in Figure 5. The region under the patch is modelled by Carver<sup>15</sup> as a thin cavity with leaking magnetic sidewalls that support quasi-discrete modes which are  $TM_{mn}$  to  $z$  ( $H_z = 0$ ) where  $m$  is the  $y$ -direction mode number and  $n$  is the  $x$ -direction mode number. The dominant radiating mode is the  $TM_{10}$  mode corresponding to the dimension  $b = \lambda_g/2$ . For the dominant mode case,  $H_z$ ,  $H_y$ , and  $E_x$  are equal to zero and  $E_z$ ,  $E_y$  and  $H_x$  are non-zero. The width of the patch  $a$  is chosen between  $b$  and  $2b$ . The electric field within the cavity is assumed to be  $z$ -directed and is given by:<sup>15</sup>

$$E_z = \sum_m \sum_n \frac{A_{mn}}{\sqrt{\epsilon abh}} e_{mn} \cos k_x x \cos k_y y, \quad (15a)$$

where

$$e_{m0} = e_{0n} = \sqrt{2}, \quad (m \neq 0 \text{ or } n \neq 0), \quad (15b)$$

$$e_{mn} = 2 \quad (m \neq 0, n \neq 0), \quad (15c)$$

and the separation equation is given as:

$$k_{10}^2 = k_x^2 + k_y^2 = \omega_{10}^2 \mu \epsilon, \quad (15d)$$

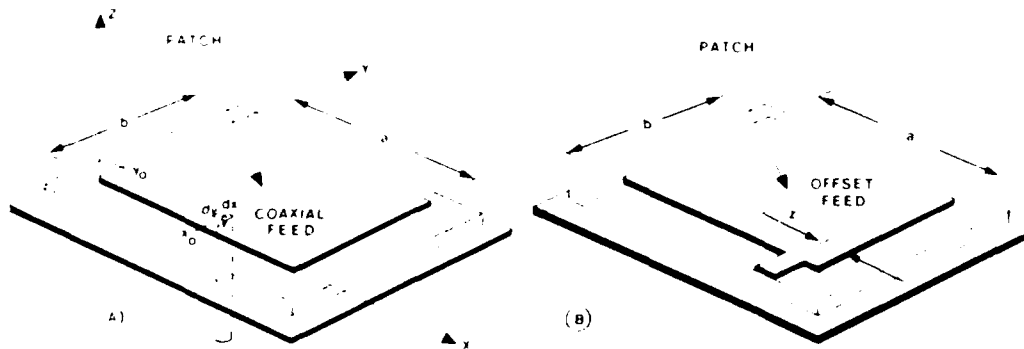


Figure 5. Probe Feed, A, and Offset Feed, B, Rectangular Patches

<sup>15</sup> Carver, K.R. (1979) Practical analytical techniques for the microstrip antenna. *Proc. Workshop on Printed Circuit Antenna Tech.*, New Mexico State Univ., Oct 1979, pp. 7/1-20.

Impedance boundary conditions are imposed at the four walls by considering the external stored and radiated energy effects as complex wall admittances. This wall admittance is equated to  $E/H$  at  $y = 0$ ,  $y = b$ ,  $x = 0$  and  $x = a$  where  $E_z$  is given by Eq. (15a) and the other field components can be computed using Maxwell's equations. This results in two equations for the determination of  $k_x$  and  $k_y$  which in turn (via Eq. (15d)) results in a complex transcendental equation for the eigenvalue  $k_{10}$  which is given by *Carver and Mink*<sup>2</sup> as:

$$\tan k_{10} b = \frac{2k_{10}\alpha_{10}}{k_{10}^2 - \alpha_{10}^2}, \quad (16a)$$

where

$$\alpha_{10} = j \frac{2\pi\eta_0 h}{\lambda_0 a} Y_w F_y(a/b), \quad (16b)$$

and the wall admittance  $Y_w$  is given as:

$$Y_w = G_w + jB_w, \quad (16c)$$

where

$$G_w = \frac{\pi}{\eta_0} \frac{a}{\lambda_0}, \quad (16d)$$

and

$$B_w = 0.01668 \frac{\Delta l}{h} \frac{a}{\lambda_0} \epsilon_{re}, \quad (16e)$$

The aspect ratio factor  $F_y(a/b)$  in Eq. (16b) is the result of an analysis by *Chang and Kuester*<sup>16</sup> which showed that the wall admittance is a function of both frequency and angle of incidence. This factor corrects the normal-incidence wall admittance given in Eq. (16c) and was empirically determined by *Carver*<sup>15</sup> as:

$$F_y(a/b) = 0.7747 + 0.5977(a/b - 1) - 0.1638(a/b - 1)^2. \quad (16d)$$

*Gogoi and Gupta*<sup>9</sup> have also computed the wall admittance at the patch edge using a Wiener-Hopf analysis<sup>17</sup> of a dielectric-loaded parallel plate waveguide with a semi-infinite bottom plate and a truncated top plate. A functional approximation of the radiation conductance based on this analysis is given as:<sup>9</sup>

$$G_s = a \left[ \frac{7.75 + 2.2k_0h + 4.8(k_0h)^2}{1000\lambda_0} \right] \left[ 1 + \frac{(\epsilon_r - 2.45)(k_0h)^3}{1.3} \right]. \quad (17a)$$

where  $\lambda_0$ ,  $a$ , and  $h$  are given in meters. This formula is claimed to have an accuracy of better than 1.1 percent for  $0.05 \leq k_0h \leq 0.6$  and  $2.45 \leq \epsilon_r \leq 2.65$ . *Gogoi and Gupta* have also developed a formula for the surface wave conductance based on this analysis which is given as:<sup>9</sup>

$$G_{sur} = ak_0h \left[ 20.493 + 65.167k_0h + 104.333(k_0h)^2 \right] 10^{-4} \\ \cdot \left[ 1 + 3.5(\epsilon_r - 2.45)(k_0h)^3 \right] \text{ mho/m}. \quad (17b)$$

Using these equations, the total wall admittance is given as  $G_w = G_s + G_{sur}$ .

The complex resonant frequency (in radians) is defined as:<sup>2</sup>

<sup>16</sup> Chang, D.C. and Kuester, E.F. (1979) Resonance characteristics of a rectangular microstrip antenna. *Proc. Workshop on Printed Circuit Antenna Tech.*, New Mexico State University, Oct 1979, pp. 28/1-18.

<sup>17</sup> Mittra, R. and Lee, S.W. (1971) *Analytical Technique in the Theory of Guided Waves*, Macmillan Co., New York.

$$\omega_{mn} = \omega_r + j\omega_l = \frac{c_0}{\sqrt{\epsilon_r - \epsilon_r j \tan \delta}} k_{10} \quad (18a)$$

where  $\tan \delta$  is the substrate dielectric loss tangent and the complex eigenvalue  $k_{10}$  is given by:<sup>2</sup>

$$k_{10} = \frac{\pi}{b} - \frac{\Delta_4}{b}, \quad (18b)$$

where the eigenvalue shift factor  $\Delta_4$  is computed by iterating the equation:

$$\Delta_{p+1} = \frac{2(\alpha_{10}b)(\pi - \Delta_p)}{(\alpha_{10}b)^2 + 2\Delta_p\pi - \Delta_p^2 - \pi^2} - \frac{\Delta_p^3}{3}, \quad p = 0, 1, 2, 3. \quad (18c)$$

with  $\Delta_0 = 0$  as the seed value. The  $\Delta_l$  in Eq. (16e) is computed using Eq. (8a). The input impedance at location  $(x_0, y_0)$  for a patch fed by a probe or a microstripline is given as:<sup>2</sup>

$$Z_{in} = -j \frac{h\omega}{\epsilon a b} \sum_{m=0}^{\infty} \sum_{n=0}^{\infty} \frac{e_{mn}^2 \cos^2(m\pi y_0/b) \cos^2(n\pi x_0/a)}{\omega^2 - \omega_{mn}^2} G_{mn} \quad (19a)$$

The term  $G_{mn}$  accounts for the finite width of the probe or the width of the microstripline and is given by:<sup>2</sup>

$$G_{mn} = \frac{\sin(m\pi d_x/2a) \sin(n\pi d_y/2b)}{m\pi d_x/2a \quad n\pi d_y/2b} \quad (19b)$$

where  $d_x = d_y$  are the probe dimensions for the probe fed case, or,  $d_x$  = microstripline width and  $d_y = 0$  for a patch fed by a microstripline at one edge (that is, dimension  $a$ ). The input impedance  $Z_{in}$  for a patch supporting only the dominant RF mode is:<sup>2</sup>



$$Z_{in} = jX_L - \frac{j(\omega/C_{10})}{\omega^2 - (\omega_r + j\omega_l)^2} \quad (20a)$$

where  $C_{10}$  is the dominant mode patch capacitance given by Reference 2 as:

$$C_{10} = \frac{\epsilon_r \epsilon_0 ab}{2h} \cos^{-2} \left( \frac{\pi y_0}{b} \right) \quad (20b)$$

and where the probe feed is represented by a lumped inductive reactance  $X_L$ , which is given by Carver and Mink<sup>2</sup> as:

$$X_L = -\frac{h}{\omega \epsilon_r \epsilon_0 ab} + \frac{\omega h}{\epsilon_r \epsilon_0 ab} \sum_{\substack{mn \neq 10 \\ mn \neq 00}}^M \sum_{\substack{N}}^N \frac{e_{mn}^2 \cos^2 \left( \frac{n\pi x_0}{a} \right) \cos^2 \left( \frac{m\pi y_0}{b} \right)}{\omega_{mn}^2 - \omega^2} G_{mn} \quad (20c)$$

A simplified equation for  $X_L$  is given by Carver:<sup>15</sup>

$$X_L = \frac{\eta_0}{\sqrt{\epsilon_r}} \tan \frac{2\pi h}{\lambda_0} \quad (20d)$$

However, when the simplified equation for  $X_L$  is used for an offset microstripline feed patch (as shown in Figure 5),  $Z_{in}$  [Eq. (18a)] must be multiplied by an offset factor  $\zeta$  which is given by Knuth and Major as:<sup>18</sup>

$$\zeta = \cos(\beta Z)^* \cos(\beta Z) \quad (21a)$$

where  $\beta = 2\pi\sqrt{\epsilon_r}/\lambda_0$  and  $Z$  is the distance from the feed point to the patch corner as shown in Figure 5.

The procedure for designing a patch using this model is:

<sup>18</sup> Knuth, E.J and Major, R.W. (1989) *Broadband Microstrip Components for EHF Steerable Antenna Arrays*. Naval Ocean Systems Center Technical Report 1278.

(i) Compute the approximate patch length  $b = 0.49\lambda_0/\sqrt{\epsilon_r}$  for the desired frequency and  $\epsilon_r$  and choose a patch width  $a$ . (for example, letting  $a = 0.65\lambda_0/\sqrt{\epsilon_r}$  will give an aspect ratio  $a/b \approx 1.3$ .)

(ii) Compute  $\Delta l$ ,  $Y_w$ , and  $F(a/b)$  using Eqs. (8a), (16c), and (16f). Compute  $\alpha_{10}$  using Eq. (16b) and iterate Eq. (18c) to find the eigenvalue shift factor  $\Delta_4$ .

(iii) Once  $\Delta_4$  is found, compute the eigenvalue  $k_{10}$  using Eq. (18b) and the resonant (radian) frequency  $\omega_r$  using Eq. (18a). The resonant frequency  $f_r = \omega_r/2\pi$ .

(iv) Compute  $G_{mn}$  using Eq. (19b), the dominant mode capacitance using Eq. (20b) and  $X_L$  using either Eq. (20c) or (20d). Now the input impedance can be computed using either Eq. (19a) or (20a).

(v) The procedure outlined in i through iv is iterated with different values of the patch length  $b$  until the desired resonant frequency is obtained.

### 3. PRACTICAL DESIGN AND MANUFACTURING CONSIDERATIONS AND CONSTRAINTS

#### 3.1 Introduction

The practical considerations of designing microstrip antennas are poorly documented. The following topics have been included in this report because I believe they play as big a part in design accuracy as model selection. Often, in fact, for the most widely used designs and fabrication techniques, (that is, single layer patches with conventional geometries and photochemical etching of copper clad substrates, respectively), *practical considerations and constraints other than model accuracy can limit the overall accuracy to such an extent that the highly complex microstrip antenna models offer little "real" improvement over some of the "simple" models.* I am not by any means implying that the complex models are overcomplicated. Indeed, there are many types of feed structures and patches for which simple models are not nearly sophisticated enough for accurate modeling. The recent generation of stacked patches that have improved bandwidth are a good example. However, complex patches of this type are only required in a small minority of applications for these antennas. The following sections contain detailed information on connectors, substrate selection and manufacturing errors, feed design and model and physical limitations as they relate to overall design accuracy.

#### 3.2 Connectors

A quick glance through the many pages of any of the popular microwave coaxial connector catalogs gives the impression that there is a wide variety of commercially available connectors for just about any microstrip design you can dream up. However, a closer look reveals that

there are only a few basic types and all of the other variations are related to mounting fixtures.

Some of the basic types of connectors used in microstrip antenna feeds and shown in Figure 6 are SMA (OSM) tab and probe connectors, and sub-miniature (OSSM) tab and probe connectors. SMA connectors allow operation from DC to 25 GHz and sub-miniature (OSSM) connectors allow operation through 38 GHz. For higher frequencies and very thin substrates (for example, 5 mil GaAs) Wiltron K and V series coaxial connectors are the most commonly used connectors. The first set of ground rules concerns tab type connectors. The width of the microstripline must be greater than the width of the tab to prevent mismatches (in this case the tab would have a lower impedance than the line), and the line width must also be smaller than the dielectric diameter to prevent shorting. Furthermore, the substrate must be thick enough so that the bottom of the center conductor of the coax portion of the connector does not short out to the ground plane of the microstripline. Finally, the difference between the widths of the tab and microstripline should be kept small to prevent a significant series inductance [Eq. (12a)] at the discontinuity. The second set of rules concerns probe connectors. Probe feeds are a very popular method for feeding microstrip antennas. When purchased, the dielectric of most commercially available probes (see Figure 6) extends out from the base of the connector to near the end of the center conductor. The dielectric must be trimmed flush with the base of the connector and a circular area with diameter equal to the connector dielectric diameter must be etched away from the ground plane before the connector is inserted. The probe center conductor is then inserted through the substrate from underneath the ground plane through a drilled hole in the substrate located at the center of the circular etched away area of the ground plane. The center conductor is then soldered to the patch antenna or to a microstripline feeding the patch antenna and the body of the connector is soldered to the ground plane. For probe feeds, the thickness of the substrate regulates the probe inductance, which can be computed using either Eq. (19) or (20d).

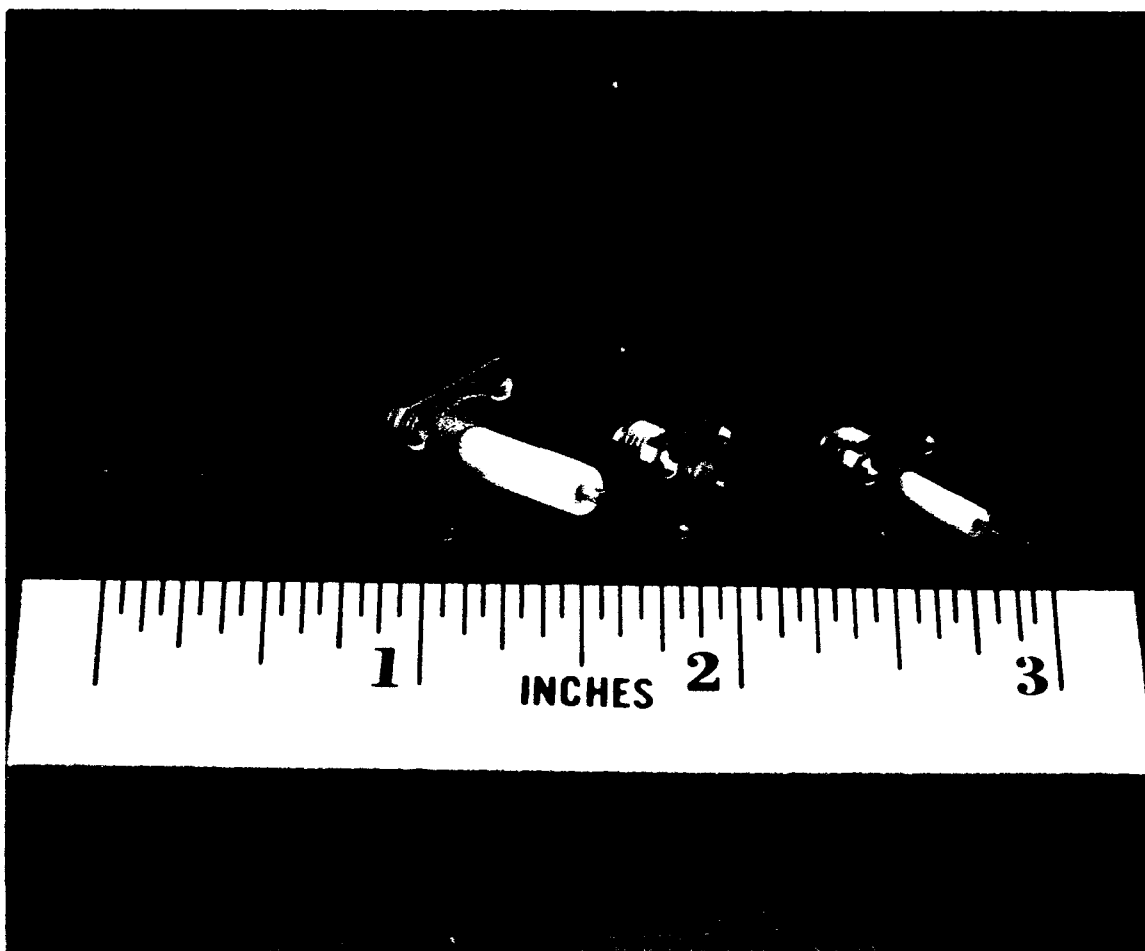


Figure 6. Common Microstrip Connectors (From left to right, SMA tab, SMA probe, OSSM tab, OSSM probe)

### 3.3 Substrate Selection and Manufacturing Errors

There are three basic substrate parameters that can be altered to suit design requirements: the dielectric constant  $\epsilon_r$ , the substrate thickness  $h$ , and the conductor or cladding thickness  $t$ . The choice of dielectric constant is usually based on space requirements in an array environment. Microstrip elements in an array are typically spaced  $0.5\lambda_0$  apart (that is, at s-band).

Since the resonant length of the antenna is approximately  $0.49\lambda_g \equiv 0.49\lambda_0/\sqrt{\epsilon_r}$ , an increase in the dielectric constant reduces the size of the patch for a given frequency, thus leaving more room in between the patch elements for feed networks, active devices, etc. Figure 7 is a plot of patch size vs frequency for three different dielectric constant materials.

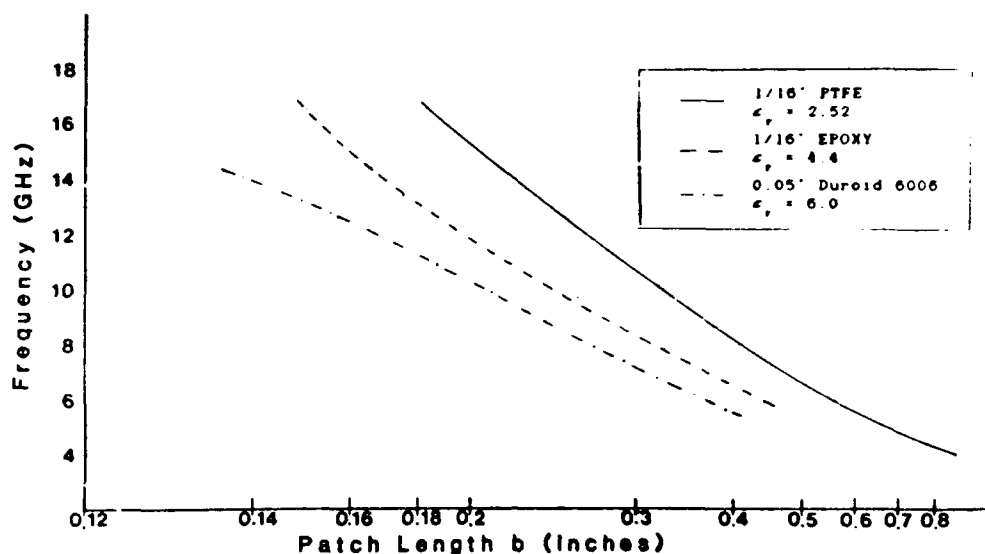


Figure 7. Microstrip Patch Size Comparison vs Frequency for  $\epsilon_r = 2.52, 4.4$  and  $6.0$

Increasing the dielectric constant also decreases the width of a microstripline for a given impedance and substrate thickness. Figure 8 shows microstripline width vs impedance for several substrates.

Higher  $\epsilon_r$  values can yield  $50\ \Omega$  lines that are narrow enough to be soldered directly to tab connectors, thus eliminating the need for input quarter wave transformers. However, it should be noted that there are many disadvantages in using high  $\epsilon_r$  substrates for patch antennas: first, the center edge impedance of a patch becomes higher as  $\epsilon_r$  increases. For example, a 4 GHz rectangular patch with an aspect ratio  $a/b \cong 1.4$  on 1/6 in. thick  $\epsilon_r = 2.52$  substrate has a center edge impedance of  $145\ \Omega$  compared to  $192\ \Omega$  for a 4 GHz patch on the same thickness  $\epsilon_r = 4.4$  material. Figure 9 gives the center edge impedances of a sample of patches ( $a/b \cong 1.4$ ) vs frequency for three different substrates as computed by the transmission line model. The combination of high patch edge impedances and narrower microstriplines at large  $\epsilon_r$  values can result in microstrip feedlines that are too narrow to fabricate due to etching tolerances.



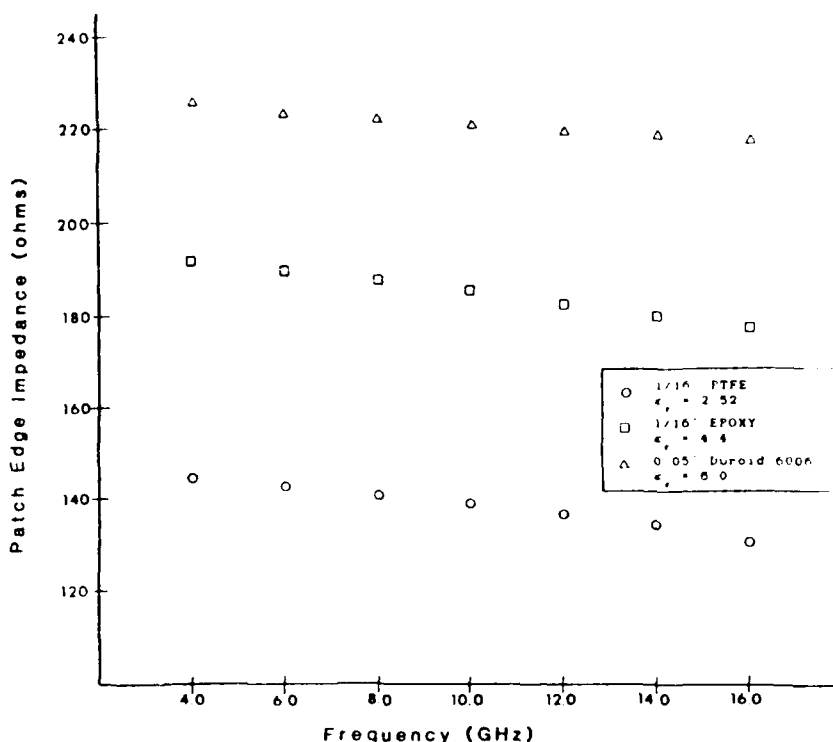


Figure 9. Rectangular Patch Center Edge Impedance vs Frequency.  $\epsilon_r = 2.52$ , 4.4, and 6.0

Second, tighter manufacturing tolerances are required on higher  $\epsilon_r$  substrates due to smaller patch sizes for a given frequency and narrower microstriplines for a given impedance. For example, on  $\epsilon_r = 2.52$  substrate, the difference between the resonant lengths of a 14 and a 16 GHz rectangular patch is 32 mils (0.032) compared to 24 mils on the same thickness of  $\epsilon_r = 4.4$  substrate. Manufacturing error consists of mask error, etching error, and error due to dielectric tolerances. The masks for printed circuit antennas are usually either photographic negatives or Rubylith. Photographic negative masks are created by generating mask artwork, usually on a pen plotter at 2 or 3 times original size, then the image is reduced before it is photographed to increase resolution. The mask error depends on plotter error, scaling factor, camera error, and error due to expansion and shrinkage of the negative, which can be as much as 3 percent. Rubylith is a much more accurate way to generate masks. Rubylith is a film coated with a double foil consisting of a clear foil and an opaque red foil. A diamond tip scribe is placed in a pen plotter or coordinatagraph and the red foil is scribed along the outline of the patch and feedlines. The red foil is then removed to create the mask. Rubylith is much thicker and thus more dimensionally stable than negatives. With an accurate pen plotter or coordinatagraph, rubylith can be cut to accuracies of less than 1 mil (20  $\mu\text{m}$ ). Substrate material for microstrip antennas is usually purchased from commercial vendors in large

sheets with copper cladding on both sides. The amount or thickness of the cladding (usually copper) is given in ounces rather than linear dimensions. "One ounce" copper cladding means one ounce of copper is spread over one square foot of area and is 0.0014 in. thick. Similarly, 1/2 ounce copper is 0.0007 in. thick and is the thinnest cladding that is available at present on commercial substrates.

Etching error is usually determined by the conductor thickness  $t$ . During the etching process, etching fluid eats away the copper covered with unexposed photoresist and leaves the copper covered with the hard, exposed photoresist. However, at the border between the exposed and unexposed photoresist, as the etching fluid eats down into the copper covered by unexposed photoresist, it also eats sideways a small amount and eats away some of the neighboring copper from underneath the exposed photoresist. This error or etching tolerance is approximately equal to the conductor thickness  $t$ . Dielectric tolerance is the variance of the substrate dielectric constant from a specified value. In general, the higher the  $\epsilon_r$ , the poorer the tolerance. Carver and Mink<sup>2</sup> give the following formula for computing the shift in frequency due to dielectric tolerance.

$$\frac{\Delta f}{f_0} = -\frac{1}{2} \frac{\delta \epsilon_r}{\epsilon_r} \quad (22a)$$

Table 1 lists the dielectric constants and tolerances of some commercially available substrates.

Table 1. Commercial Substrate Tolerances

Substrate	Dielectric Tolerance $\epsilon_r$
RT/duroid 5880	2.20 $\pm$ 0.02
RT/duroid 5870	2.33 $\pm$ 0.02
OAK-605	2.20 $\pm$ 0.02
OAK-605	2.33 $\pm$ 0.02
TACONIC TLY-5	2.20 $\pm$ 0.02
TACONIC TLY-3	2.30 $\pm$ 0.02
RT/duroid 5500	2.50 $\pm$ 0.04
OAK-602	2.50 $\pm$ 0.02
TACONIC TLX	2.50 $\pm$ 0.04
RT/duroid 6006	6.00 $\pm$ 0.15
RT/duroid 6010	10.50 $\pm$ 0.25
Epsilam-10	10.30 $\pm$ 0.50



Third, some high  $\epsilon_r$  substrates have uniaxial dielectric constants. Epsilam-10 has a dielectric constant of 10.3 in the z-direction and a dielectric constant of "approximately 15" in the x and y directions. RT/duroid only lists a z-direction dielectric constant for their 6006 and 6010 material, which suggests these materials may be uniaxial as well.

Finally, higher dielectric constant substrates tend to produce microstrip patch antennas with less bandwidth than the electrical thickness of the patch would suggest. The theoretical (cavity model) 2:1 VSWR bandwidth of patch antennas on  $\epsilon_r = 2.52$ , 4.4, and 6.0 material is given in Figure 10. Bandwidth at the lower frequencies is dictated by the dielectric constant, electrical thickness, and the loss tangent of the material. From Figure 10, first note that for a given material, the bandwidth increases with increasing frequency. This is due to the increasing electrical thickness of the substrate with increasing frequency and it makes sense because the  $Q$  of the patch goes down with increasing substrate thickness. Second, note that for different materials at a given frequency, for example, the  $\epsilon_r = 6.0$  and 2.52 materials at 8 GHz, the substrates have similar loss tangents (0.0027 and 0.0019, respectively), yet the  $\epsilon_r = 6.0$  patch has lower bandwidth, even though it is electrically thicker. This is due to the higher  $\epsilon_r$ , which in turn increases  $Q_r$ . Finally, the effects of loss tangent can be seen by looking at the bandwidth of the  $\epsilon_r = 4.4$  material in Figure 10. This material has a much higher loss tangent ( $\tan \delta = 0.025$ ) than the other materials. From the figure, patches on this material have more bandwidth than the dielectric constant and electrical thickness suggest. However, the bandwidth increase in this case is caused by dielectric losses. Carver and Mink<sup>2</sup> give the following series of equations for computing the theoretical bandwidth and efficiency for a patch antenna:

$$BW = \frac{\Delta f}{f} = \frac{VSWR - 1}{Q \sqrt{VSWR}} \quad (23a)$$

where

$$Q = \frac{1}{Q_r} + \frac{1}{Q_d} + \frac{1}{Q_t} \quad (23b)$$

and

$$Q_t = \frac{R_r(k_{10})}{2Im(k_{10})} \text{ is the } Q\text{-factor due to radiation losses;} \quad (23c)$$

$$Q_d = \frac{1}{\tan \delta} \text{ is the } Q\text{-factor due to dielectric losses;} \quad (23d)$$

$$Q_c = \frac{h}{\delta_s} \text{ is the } Q\text{-factor due to conductor losses;} \quad (23e)$$

$$\delta_s = \frac{1}{\sqrt{\pi f \mu_0 \sigma}} \text{ is the skin depth.} \quad (23f)$$

where  $\tan \delta$  is the loss tangent of the dielectric,  $\mu_0$  is the free space permeability,  $\sigma$  is the conductivity and  $k_{10}$  is the eigenvalue computed using the cavity model.

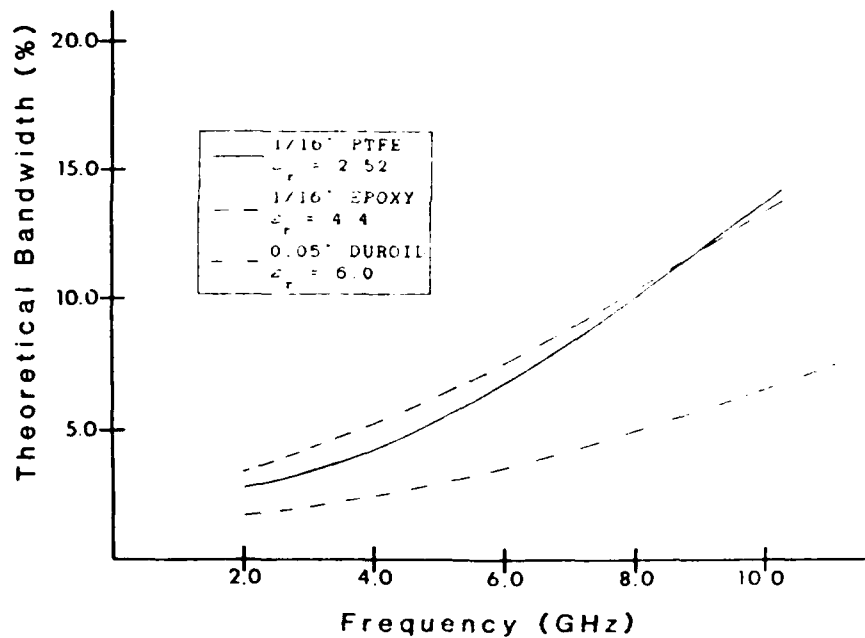


Figure 10. Theoretical 2:1 VSWR Bandwidth vs Frequency

The efficiency  $\eta$  of these antennas depends primarily on the loss tangent and the electrical thickness of the substrate. The efficiency  $\eta$  of a microstrip antenna is given by<sup>2</sup> as:

$$\eta = \frac{\text{Power Radiated}}{\text{Power Input}} = \frac{G_{\text{rad}}}{G_{\text{in}}} \quad (24a)$$

where

$$G_{\text{in}} = G_{\text{rad}} + G_{\text{cu}} + G_{\text{dl}} \quad (24b)$$

$$G_{\text{rad}} = \frac{\omega C_{10}}{Q_r} \quad (24c)$$

$$G_{\text{cu}} = \frac{(\mu\omega/2\sigma)^{1/2} \pi^2 a}{2\omega^2 \mu^2 b h} \quad (24d)$$

and

$$G_{\text{dl}} = \omega C_{10} \tan \delta \quad (24e)$$

For most microstrip antennas, the efficiency is more than 90 percent. Generally, electrically thinner substrates and higher loss tangents combine for lower efficiency as shown in Figure 11.

Changing the thickness of the substrate  $h$  also changes the distance that the fringing fields extend away from the edge of the patch. The net result is that for a given frequency and dielectric constant, decreasing  $h$  will make the fringing field length extension slightly smaller and thus the patch size will be slightly larger. Increasing the thickness of the substrate  $h$  increases the distance that the fringing fields extend away from the patch edge thus making the patch slightly smaller for a given frequency and  $\epsilon_r$ .

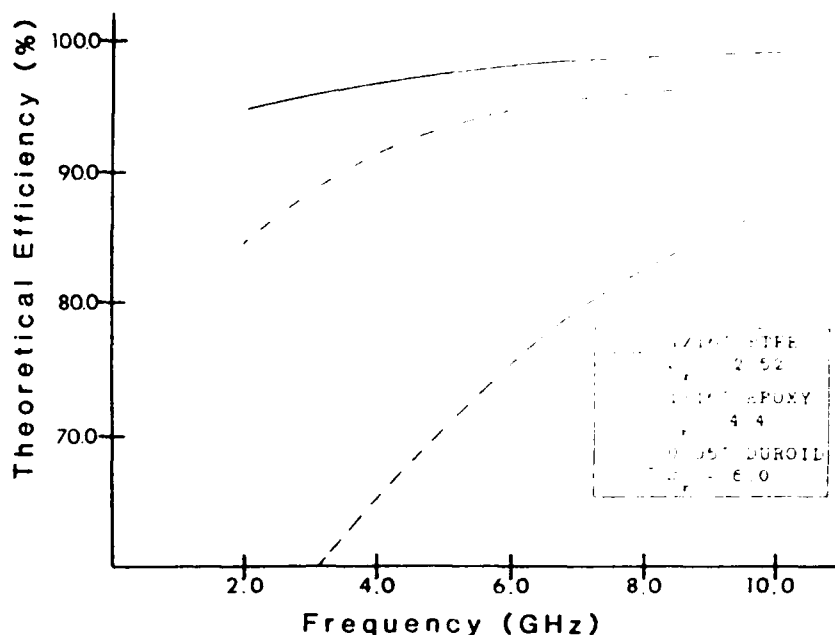


Figure 11. Rectangular Microstrip Patch Efficiency

### 3.4 Feed Design (Transformer vs Inset vs Probe vs Offset)

The general design of the feed network is usually determined by the application, and then the specific design is driven by additional constraints imposed by the model, connectors, substrate, manufacturing error, and operating frequency.

Probe feeds are used most often in applications where the antenna is to be flush mounted on the surface and fed from behind. This type of feed is shown in Figure 5. They can be soldered directly to the patch from underneath thus forming a simple and efficient feeding technique. However, the series inductance associated with this feed and mentioned earlier increases with increasing electrical substrate thickness. While this inductance is easy to compute for thin substrates using Eq. (18d), the rigorous solution (Eq. 18c) converges very slowly and is difficult to compute. Furthermore, this type of feed cannot be used with the transmission line model without modification because the probe inductance is not accounted for (the transmission line model assumes a real feedline impedance).

Transformer edge feeds, offset feeds, and the inset feeds are shown in Figures 1, 5 and 12 respectively. They are most often used in single elements or in arrays that use a microstripline feed network. Transformer edge feeds are the most common. In this case, a  $\lambda_g/4$  microstrip impedance transformer is used to feed the patch edge. The impedance of this transformer is (see Figure 1)  $Z_{u12} = \sqrt{\bar{Z}_{u1} \bar{Z}_{in}}$  where  $Z_{in}$  is the patch edge impedance. The patch edge impedance (see Figure 9), manufacturing tolerances (see Table 2) and microstripline

widths (see Figure 8) determine whether an impedance transformer is needed here. The lines could be too thin to fabricate accurately. Another impedance transformer may be required at the substrate edge depending on the connector dimensions and the impedance of the microstripline at the substrate edge. For example, an Omni-Spectra SMA tab connector (P/N 2052-1618-00) like the one shown in Figure 6 has a tab 0.05 in. wide by 0.1 in. long and the diameter of the connector dielectric is 0.162 in. If a 50  $\Omega$  microstripline is wider than 0.162 in. or narrower than 0.05 in. then a microstripline impedance transformer will be needed where (Refer to Figure 1)  $Z_{ut} = \sqrt{50Z_{ut}}$  (50 $\Omega$  is the assumed tab or probe connector impedance). This impedance transformer is then soldered to the connector at the substrate edge. An intermediate impedance line whose length is  $n\lambda_g/2$  completes the feed design by connecting the two transformers while maintaining a purely real impedance. The impedance transformer at the patch feed can be eliminated through the use of either an offset or an inset feed. An offset feed is shown in Figure 5. The impedance at the offset location can be computed using either Eq. (19a) or Eqs. (20a) and (21a) in conjunction with the cavity model. The impedance at the offset location cannot be computed using a transmission line model. However, an inset feed patch as shown in Figure 12 can be modelled with either a transmission line or cavity model. In a rectangular patch, the real part of the input impedance has a high value at the radiating edge and goes to zero at the patch center (the  $TM_{10}$  mode has a zero crossing at the center). By cutting two small slots of length  $d$  and width  $s$  adjacent to and on both sides of the feedline, the feedpoint impedance can be lowered to a value which corresponds to the desired feedline impedance. The depth of the inset  $d$  is derived from an expression given by Carver and Mink<sup>2</sup> and is given approximately by the expression:

$$d \cong (b/\pi) \cos^{-1} \sqrt{\frac{R_0}{R_e}} \quad (25a)$$

where  $R_0$  is the feedline characteristic resistance and  $R_e$  is the edge resistance of the patch without the inset feed. The transmission line model can be used to determine  $d$  more accurately by substituting  $x_1 = ka \sqrt{\epsilon_{re}} + ka$  for Eq. (11c) and iterating Eq. (11a) until the imaginary part of the input impedance is zero and the real part equals the feedline resistance.

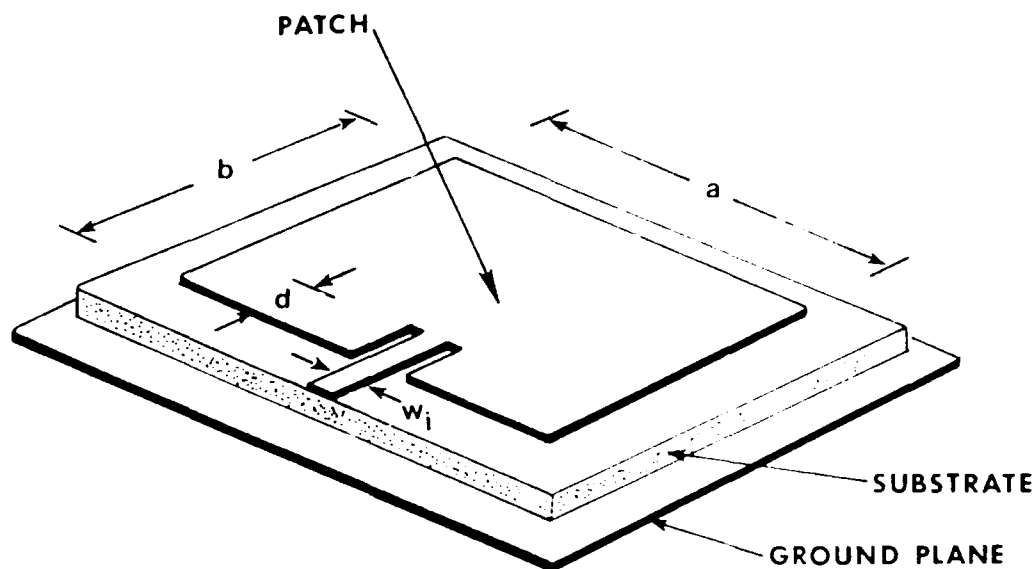


Figure 12. Inset Feed Rectangular Patch

Table 2. Surface Wave Mode Cutoff Frequencies

Material, $\epsilon_r$	$h$ (in.)	$F_c$ (Ghz)		
		TE <sub>1</sub>	TM <sub>2</sub>	TE <sub>3</sub>
PTFE, 2.54	0.0625	38.04	76.09	114.13
PTFE, 2.54	0.125	19.02	38.04	57.06
Epsilam 10, 10.0	0.025	39.34	78.69	118.03
Epsilam 10, 10.0	0.050	19.67	39.34	59.01
GaAs, 12.8	0.004	214.75	429.49	644.24
GaAs, 12.8	0.010	85.90	171.80	257.70

### 3.5 Model and Physical Limitations

In previous sections of this report, we saw that increasing the thickness of the substrate yields improvements in bandwidth. Since narrow bandwidth is so undesirable in microstrip antennas, one might ask why thick substrates are not used. Model and physical limitations are the reason. A substrate thickness of  $0.25 \lambda_g$  is one clear and obvious limitation, since feed lines and feed probes become antennas themselves, resulting in distorted, unpredictable patterns. A patch with this substrate thickness would have about 20 percent bandwidth which

is considered to be fairly wide band. Unfortunately, there are many additional constraints that come into play depending on the model used, the type of feed, the substrate material, and the environment the antenna is placed in that limit the thickness to much less than  $0.25 \lambda_g$ . The first constraints are model constraints. For the transmission line model, both sets of slot admittance equations have substrate thickness validity constraints. Equation (2a) is limited to substrates with  $h \leq 0.1 \lambda_g$  and Eq. (4a) is limited to  $h \leq 0.048 \lambda_g$ . The cavity model has similar constraints since it assumes the E-field of the patch interior is Z-directed only. The literature is vague with regard to an actual number for this model, but again  $h \leq 0.1 \lambda_g$  is a reasonable number. The excitation of surface wave modes imposes additional limitations on substrate thickness, especially if the patch antenna is an element in an electronic scanning (phased) array. Surface waves are *TE* and *TM* modes which propagate outside of the patch into the substrate. A strong coupling can occur if the phase velocity of the quasi-*TEM* mode in the patch is less than the phase velocity of the surface wave, resulting in reduced efficiency in single elements or "blind spots" in array patterns for certain frequencies or when an array is scanned to certain angles. For single elements, Harrington's<sup>7</sup> analysis of dielectric coated conductors gives the cutoff frequencies of the surface wave modes as:

$$f_c = \frac{n c_0}{4h \sqrt{\epsilon_r - 1}} \quad (26a)$$

where  $c_0$  is the speed of light in free space and  $n = 0, 2, 4, \dots$  for *TM* modes and  $n = 1, 3, 5, \dots$  for *TE* modes. There is no cutoff for the *TM*<sub>0</sub> mode. McGrath and Fitzgerald<sup>19</sup> list the cutoff frequencies for some higher order modes and popular substrates in Table 2. Fortunately, the table indicates that higher order surface waves modes for single elements only manifest themselves in cases where  $h \approx 0.3 \lambda_g$  or greater. The *TM*<sub>0</sub> mode is the only mode that presents a problem. As the substrate thickness increases, more energy is coupled into this mode resulting in lower patch efficiency. Gogoi and Gupta<sup>9</sup> have found that the reduction in efficiency due to surface waves becomes significant for substrate thicknesses  $h \geq 0.048 \lambda_0$  and at  $h = 0.12 \lambda_0$ , the surface wave conductance [Eq. (17b)] is equal to the radiation conductance.

Dispersion is a material phenomenon in microstrip where the relationship between the frequency and propagation velocity is not linear and  $\epsilon_{re}$  becomes a function of frequency. Woernbke<sup>20</sup> gives a critical frequency (GHz) above which dispersive effects become significant as:

$$f_c = 0.3 \cdot Z_c / 2.54h (\epsilon_r - 1)^{1/2} \quad (27a)$$

<sup>19</sup> McGrath, D.T. and Fitzgerald, M.R. (1987) *Investigation of Surface Wave Blindness in Microstrip Phased Array Antennas*, RADC In-House Report RADC-TR-87-39, ADA189326.

<sup>20</sup> Woernbke, J.D. (1982) Soft substrates conquer hard designs, *Microwaves*, January 1982.

From the equation above, patches with large aspect ratios  $a/b$ , thick substrates, and high  $\epsilon_r$  values are most prone to dispersion. For these conditions the effective dielectric constant becomes:<sup>20</sup>

$$\epsilon_{re}(f) = \epsilon_r - \left[ \frac{\epsilon_r - \epsilon_{re}}{1 + G(f/f_p)^2} \right], \quad (28a)$$

where

$$f_p = Z_c/2\mu h, \quad (28b)$$

and

$$G = 0.6 + 0.009Z_c. \quad (28c)$$

## 4. EXPERIMENTAL RESULTS AND DISCUSSION

### 4.1 Introduction

For comparison purposes, three sets of rectangular patches were constructed on three different dielectric constant substrates: 1/16 in.-thick PTFE ( $\epsilon_r = 2.52$ ,  $t = 0.0007$ ,  $\tan \delta = 0.0019$ ), 1/16 in.-thick G10 Epoxy ( $\epsilon_r = 4.4$ ,  $t = 0.0014$ ,  $\tan \delta = 0.025$ ) and 0.05 in.-thick 6006 Duroid ( $\epsilon_r = 6.0$ ,  $t = 0.0007$ ,  $\tan \delta = 0.0027$ ). Each set consists of seven patches with resonant frequencies between 4 and 16 GHz. Seven stagger tuned patches were also constructed on 1/16 in.-thick PTFE. Figures 13a-d contain photos showing one of the patches from each set. Since the radiation patterns of rectangular patch antennas have been studied extensively



and are given in many references<sup>21,22,23</sup> pattern measurements will not be presented here. However, extensive measurements of patch resonant frequencies and input impedance are given in Appendix A for all of the rectangular patches and in Appendix B for all of the stagger tuned patches. In addition, precise manufacturing error measurements will be given later in this section for all measured patches.

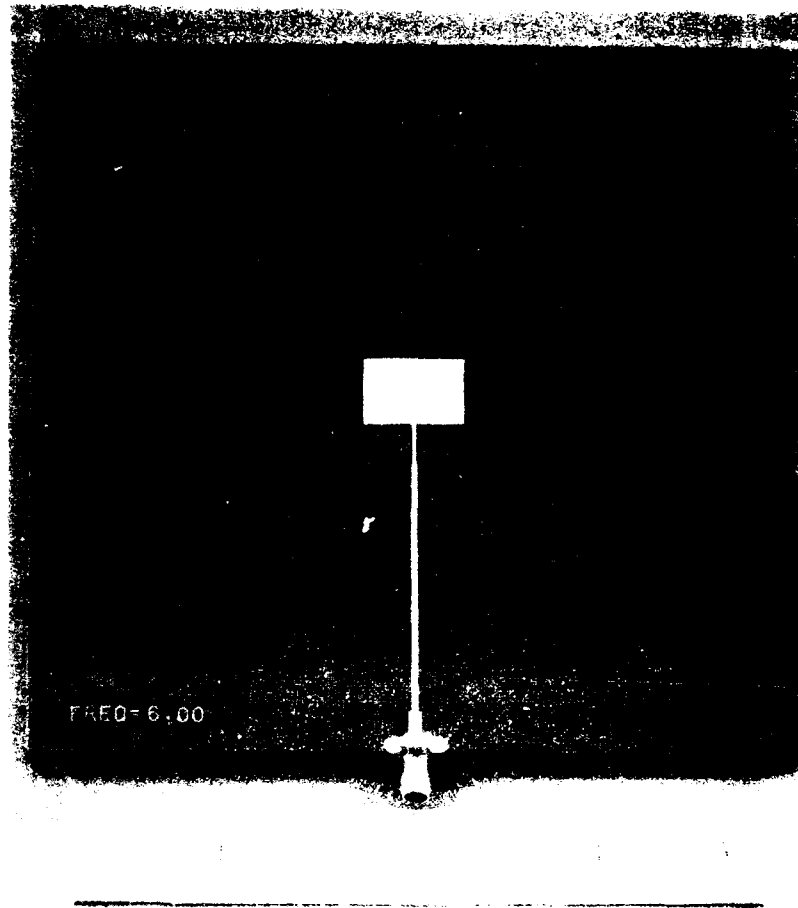


Figure 13a. Rectangular Patch On  $\epsilon_r = 2.52$

<sup>21</sup> Bahl, I.J. and Bhartia, P. (1980) *Microstrip Antennas*, Artech House.

<sup>22</sup> Gupta, K.C. and Benalla, A. (1988) *Microstrip Antenna Design*, Artech House.

<sup>23</sup> James, J.R., Hall, P.S., and Wood, C. (1981) *Microstrip Antenna Theory and Design*, Peter Peregrinus Ltd.

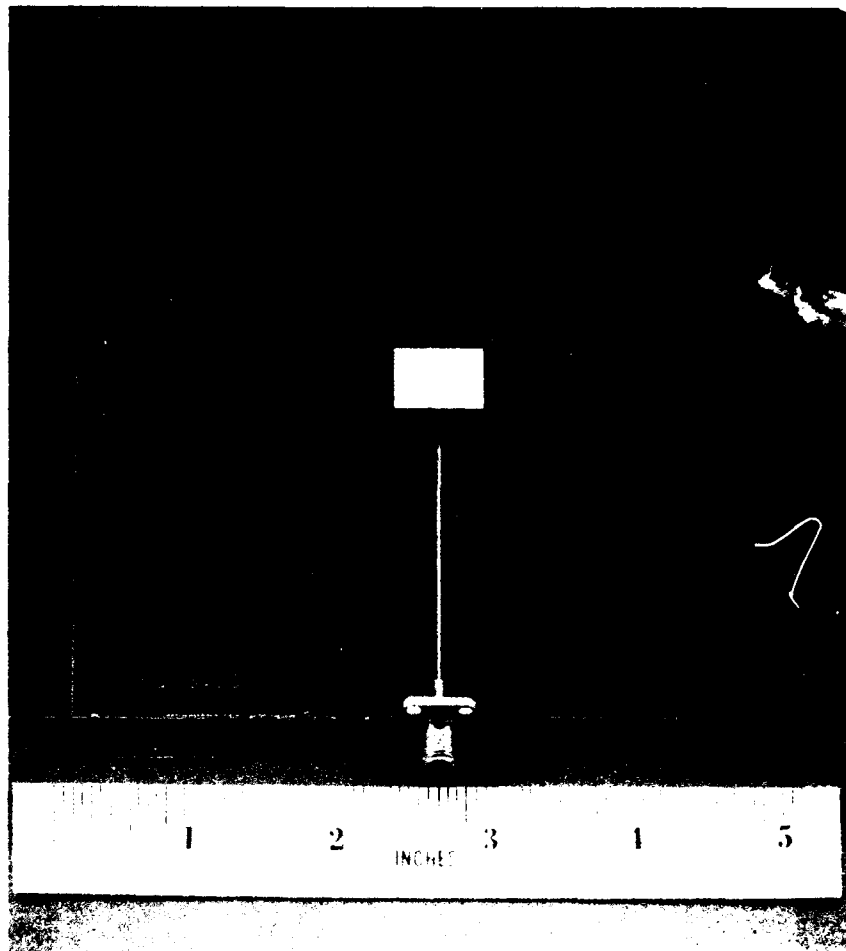


Figure 13b. Rectangular Patch on  $\epsilon_r = 4.4$

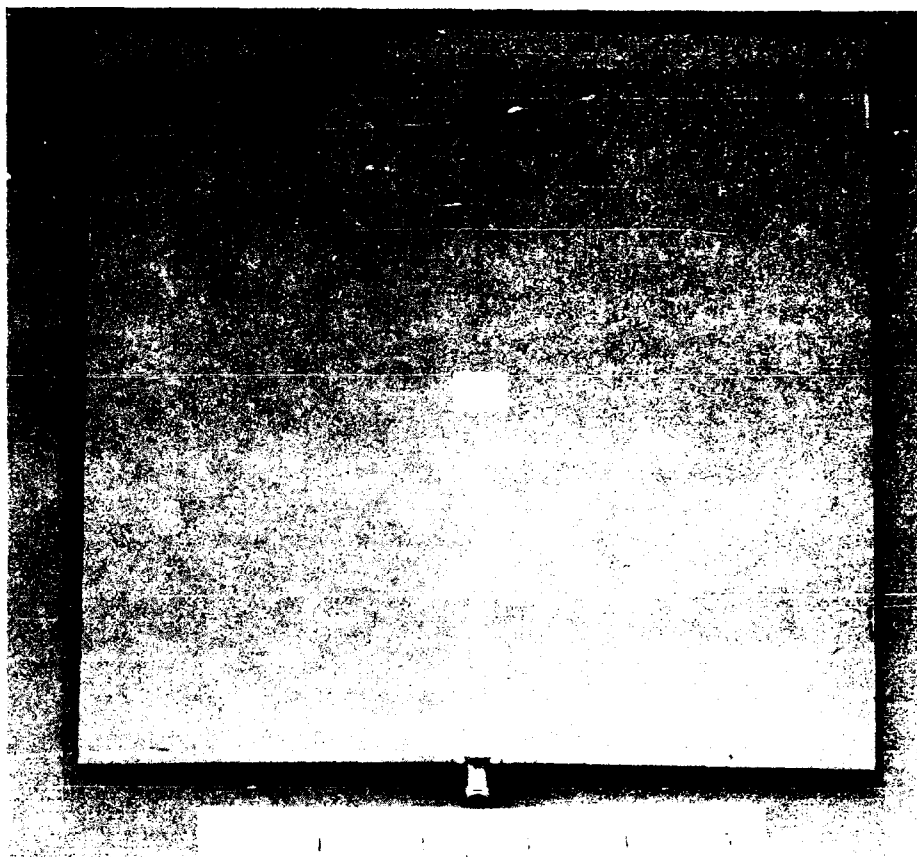


Figure 13c. Rectangular Patch on  $\epsilon_r = 6.0$

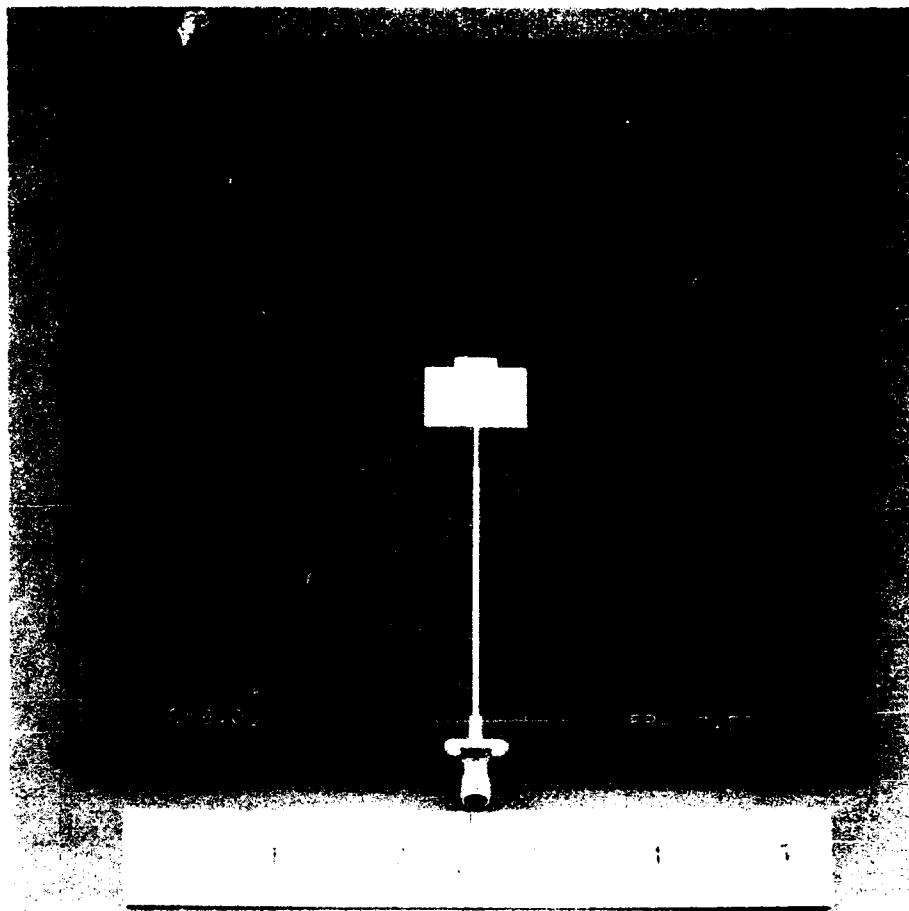


Figure 13d. Stagger Tuned Patch on  $\epsilon_r = 2.52$

#### 4.2 Manufacturing Error

Before models can be compared, the actual patch dimensions must be measured precisely. This yields information on the manufacturing error and also allows the model comparison to be based on actual patch dimensions rather than what the dimensions were supposed to be. The dimensions of all four sets of patches were measured using a Mitutoyo PH-350 profile projector comparator which is accurate to 0.0001 in. The masks were generated by first plotting the mask artwork on a Calcomp 1055 drum plotter at a 2x scale factor. The mask was then taken to a photo lab and photographed at a 50 percent reduction. The mask itself is a standard photographic negative. The measured dimensions of all of the patches are given in Table 2 and the percent error in the resonant patch length  $b$  vs frequency is given for all patch sets in Figure 14. There are three patches missing from the four sets. The 14 GHz,

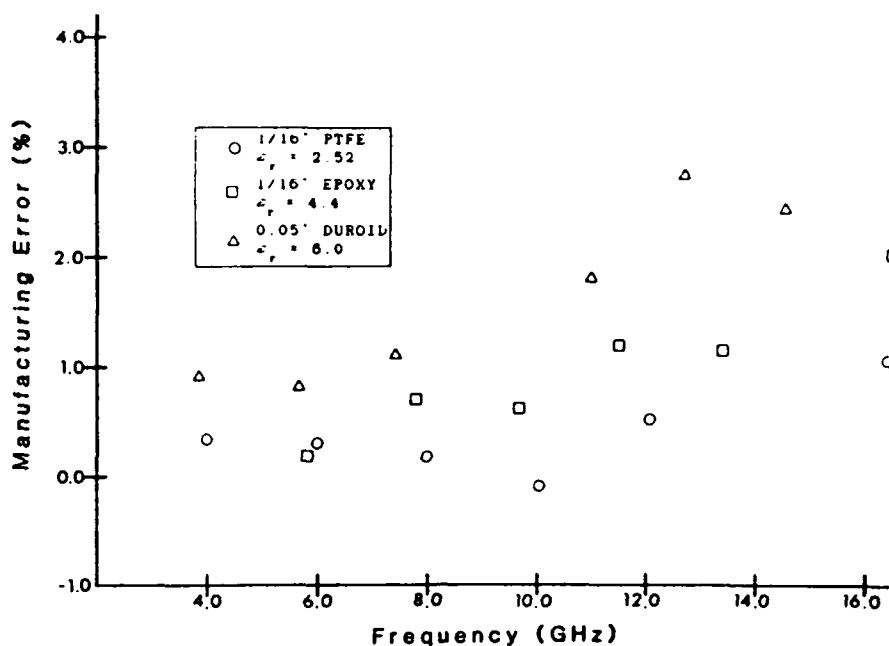


Figure 14. Manufacturing error vs Frequency

$\epsilon_r = 2.52$  mask and the 10 GHz,  $\epsilon_r = 6.0$  mask were interchanged by our etching contractor and etched on the wrong material, rendering them useless. Also, the patch input transformer for the 4 GHz,  $\epsilon_r = 4.4$  patch was etched away entirely. Note that while the etching error in Table 3 remains about the same, the manufacturing percent error in Figure 14 rises considerably with increasing frequency and  $\epsilon_r$ , due to an increasingly smaller resonant length  $b$ . As mentioned earlier, the etching error on each edge of a microstripline can be as much as the thickness of the conductor,  $t$ . Since nearly all of the measured patch dimensions were smaller than the design dimensions, we conclude that the mask error was small and most of the manufacturing error is due to etching errors. The few cases where the measured dimensions are bigger is probably due to plotter error since the other measured dimensions on the same patch followed the norm and were smaller than the design dimensions. Unfortunately, the only way to reduce etching error is to wait for substrates to come out with thinner conductors or use a different manufacturing technique such as the techniques currently used in MMICs (Monolithic Microwave Integrated Circuits) where the metalization is laid down on the substrate rather than being etched off.

Table 3. Manufacturing Tolerances

Rectangular patches							
Measured Freq (GHz)	$\epsilon_r$	Design $a$ (in.)	Measured $a$	Design $b$ (in.)	Measured $b$	Design $W_{t2}$ (in.)	Measured $W_{t2}$
3.99	2.52	1.2082	1.2083	0.8651	0.8622	0.0297	0.0259
5.98	2.52	0.8054	0.8021	0.5600	0.5583	0.0301	0.0265
8.00	2.52	0.6041	0.6037	0.4082	0.4075	0.0307	0.0278
10.06	2.52	0.4833	0.4830	0.3176	0.3179	0.0314	0.0310
12.16	2.52	0.4027	0.3996	0.2576	0.2562	0.0322	0.0289
16.40	2.52	0.3020	0.3007	0.1832	0.1813	0.0339	0.0310
5.88	4.4	0.6096	0.6095	0.4449	0.4441	0.0076	0.0064
7.82	4.4	0.4572	0.4561	0.3278	0.3255	0.0078	0.0074
9.66	4.4	0.3657	0.3649	0.2576	0.2560	0.0080	0.0057
11.50	4.4	0.3048	0.3015	0.2108	0.2083	0.0082	0.0061
13.37	4.4	0.2612	0.2579	0.1774	0.1754	0.0085	0.0061
16.46	4.4	0.2286	0.2260	0.1525	0.1495	0.0088	0.0058
3.86	6.0	0.7830	0.7777	0.5944	0.5890	0.0100	0.0099
5.64	6.0	0.5220	0.5186	0.3927	0.3895	0.0100	0.0075
7.43	6.0	0.3915	0.3878	0.2917	0.2885	0.0102	0.0081
10.94	6.0	0.2610	0.2565	0.1903	0.1869	0.0104	0.0076
12.66	6.0	0.2237	0.2201	0.1613	0.1570	0.0106	0.0049
14.27	6.0	0.1958	0.1918	0.1395	0.1362	0.0107	0.0060
Stagger Tuned Patches							
Measured Freq (GHz)	$\epsilon_r$	Design $w_1$ (in.)	Measured $w_1$	Design $l_1$ (in.)	Measured $l_1$	Design $W_{t2}$ (in.)	Measured $W_{t2}$
4.00	2.52	1.2082	1.2059	0.7913	0.8135	0.0303	0.0260
6.02	2.52	0.8055	0.8045	0.5015	0.5032	0.0309	0.0269
8.17	2.52	0.6041	0.6016	0.3629	0.3609	0.0314	0.0272
10.28	2.52	0.4833	0.4823	0.2782	0.2760	0.0320	0.0277
12.46	2.52	0.4027	0.4004	0.2221	0.2197	0.0326	0.0292
14.66	2.52	0.3452	0.3431	0.1823	0.1791	0.0333	0.0298
16.93	2.52	0.3021	0.2990	0.1526	0.1503	0.0340	0.0312
Measured Freq (GHz)	$\epsilon_r$	Design $w_2$ (in.)	Measured $w_2$	Design $l_2$ (in.)	Measured $l_2$		
4.00	2.52	0.5074	0.5045	0.1275	0.1250		
6.02	2.52	0.3383	0.3347	0.0850	0.0862		
8.17	2.52	0.2537	0.2512	0.0638	0.0639		
10.28	2.52	0.2030	0.1999	0.0510	0.0503		
12.46	2.52	0.1691	0.1679	0.0425	0.0411		
14.66	2.52	0.1450	0.1423	0.0364	0.0361		
16.93	2.52	0.1269	0.1257	0.0319	0.0314		

#### 4.3 Rectangular Patch Measurement Results

As the reader recalls, three sets of transformer fed rectangular patches were constructed on different  $\epsilon_r$  substrates with resonant frequencies between 4 and 16 GHz. In the last section, the measured physical dimensions of these patches recorded and the manufacturing errors were determined. The resonant frequency of each patch was measured on an HP 8510 network

analyzer and these data are documented in Appendix A. In this section, the measured results will be compared to transmission line model results using different combinations of equations and the measured data will also be compared to Carver's modal expansion cavity model predictions. Figures 15 through 17 give the model error vs resonant frequency for each set of patches. The original transmission line model uses Eq. (4a) for  $Y_S$  with  $\lambda_g = \lambda_0/\sqrt{\epsilon_r}$  and  $Y_C$  is given by Munson<sup>1</sup> as:

$$Y_C = \frac{\alpha \sqrt{\epsilon_r}}{h \eta_0} \quad (29a)$$

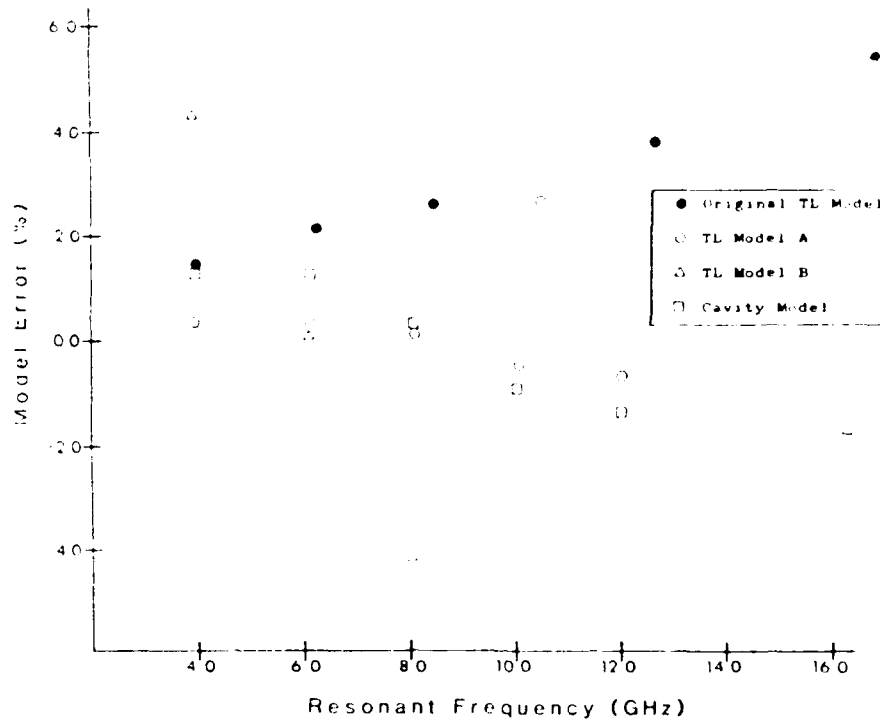


Figure 15. Model Error vs Resonant Frequency,  $\epsilon_r = 2.52$

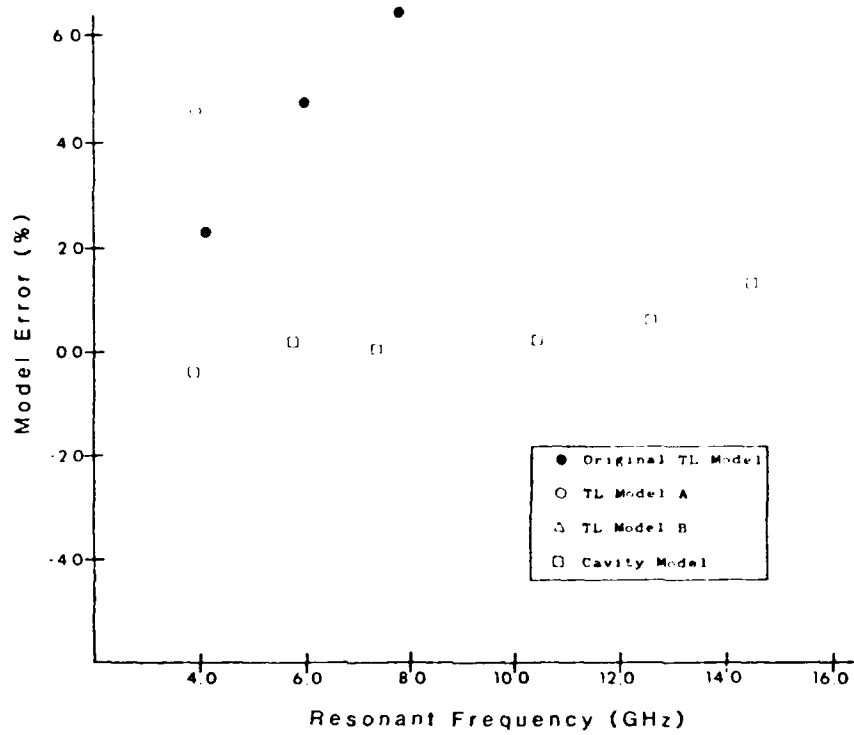


Figure 16. Model Error vs Resonant Frequency.  $\epsilon_r = 6.0$



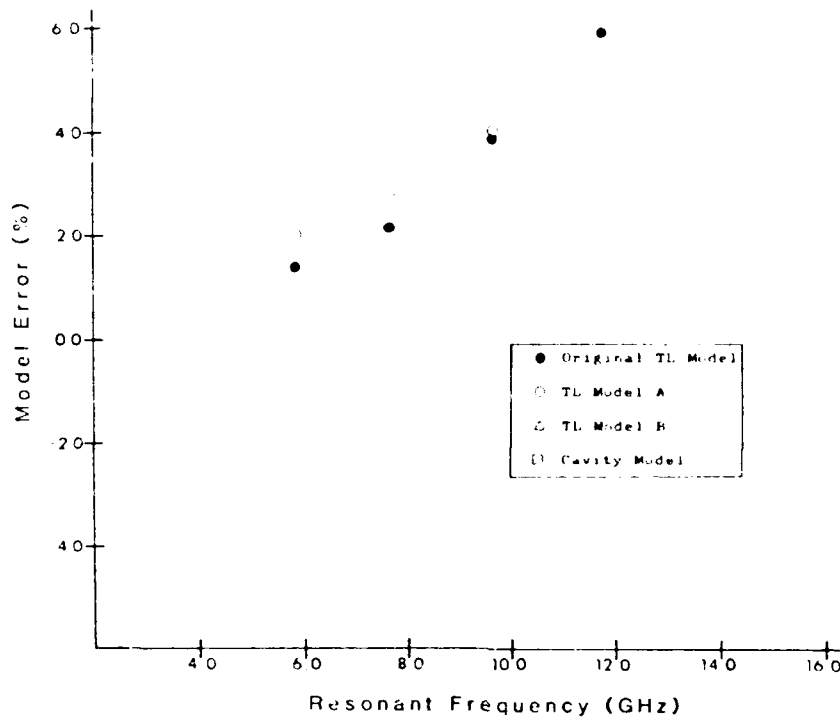


Figure 17. Model Error vs Resonant Frequency,  $\epsilon_r = 4.4$

TL Model A is the transmission line model as defined in Section 3.1 with Eqs. (1a), (1c), (4a), and (8a) for the patch admittance, effective dielectric constant, slot admittance, and length extension, respectively. TL Model B is also the transmission line model as described in Section 3.1 but uses Eqs. (3a), (3c), (6a) and (6b), and (9a) for the above parameters, respectively.

Figure 15 shows the results from set 1 ( $\epsilon_r = 2.52$ ). TL Model A performed very well. The average error (error = (model frequency - measured frequency)/measured frequency) between the model and measured frequencies was only 0.7 percent compared to 3 percent for the original model. From Appendix A, the return loss values for all of the patches in this set indicate that the model was also accurate in predicting the feedpoint impedance. The return loss is defined as  $RL = 20 \log |\Gamma|$  where  $\Gamma$  is the reflection coefficient and the normalization impedance of the Smith Chart data is  $50 \Omega$ . The modal expansion cavity model also did well for this set with an average resonant frequency model error of 1.19 percent. This model also accurately predicts the input impedance as evidenced by the measured return losses and Table 4. However, TL Model B did not perform so well. The validity region of Eq. (6a) is  $h \leq 0.048 \lambda_g$  which corresponds to only 6 GHz on this material. From Figure 15, you can see that in the region around 6 GHz, it performed well, but at most other frequencies it wasn't even on the scale.

Table 4. Rectangular Patch Input Impedances

Measured Freq. (GHz)	$\epsilon_r$	TL Model A	Cavity Model
3.99	2.52	145.1 $\Omega$	145 + j29 $\Omega$
5.98	2.52	143.5 $\Omega$	144 + j44 $\Omega$
8.00	2.52	141.5 $\Omega$	138 + j59 $\Omega$
10.06	2.52	139.2 $\Omega$	131 + j76 $\Omega$
12.16	2.52	136.9 $\Omega$	126 + j93 $\Omega$
16.40	2.52	131.5 $\Omega$	114 + j132 $\Omega$
3.86	6.00	225.3 $\Omega$	234 + j13 $\Omega$
5.64	6.00	224.3 $\Omega$	250 + j20 $\Omega$
7.43	6.00	223.2 $\Omega$	256 + j26 $\Omega$
10.94	6.00	220.3 $\Omega$	260 + j39 $\Omega$
12.66	6.00	218.7 $\Omega$	258 + j46 $\Omega$
14.27	6.00	217.1 $\Omega$	260 + j52 $\Omega$
5.88	4.4	190.1 $\Omega$	149 + j32 $\Omega$
7.82	4.4	188.1 $\Omega$	157 + j43 $\Omega$
9.66	4.4	185.8 $\Omega$	161 + j53 $\Omega$
11.50	4.4	183.4 $\Omega$	165 + j63 $\Omega$
13.37	4.4	180.8 $\Omega$	161 + j74 $\Omega$
16.46	4.4	178.2 $\Omega$	117 + j96 $\Omega$

For set 2 ( $\epsilon_r = 6.0$ ), none of the transmission line models performed well. The average resonant frequency model error for TL Model A was 10 percent and TL Model B at most frequencies had greater than 10 percent error. On the other hand, the cavity model performed even better on this set than in set 1 as seen in Figure 16 with an average resonant frequency error of only 0.64 percent. The return loss values for the patches in this set were good up to about 12 GHz after which they became much poorer. All of these patches were originally designed using a transmission line model. Since the actual resonant frequency was more than 10 percent lower than the original design frequency, the poor return loss is probably due to the transformer being out of band with the patch.

None of the models did well in predicting the resonances for set 3 ( $\epsilon_r = 4.4$ ) as seen in Figure 17. The original transmission line model and TL Model A did the best with  $\approx 1.5$  percent error at 6 GHz but the error quickly became much worse for higher frequencies. Since none of the models were accurate for this substrate, I suspect the dielectric constant of this sheet was not at the assumed value. Also, I believe that the measured resonance at 16.46 GHz is an error and that something else is resonating other than the patch. The measured 2:1 VSWR bandwidth of

all of the patch sets is shown in Figure 18 and generally follows the theoretical data of Figure 10.

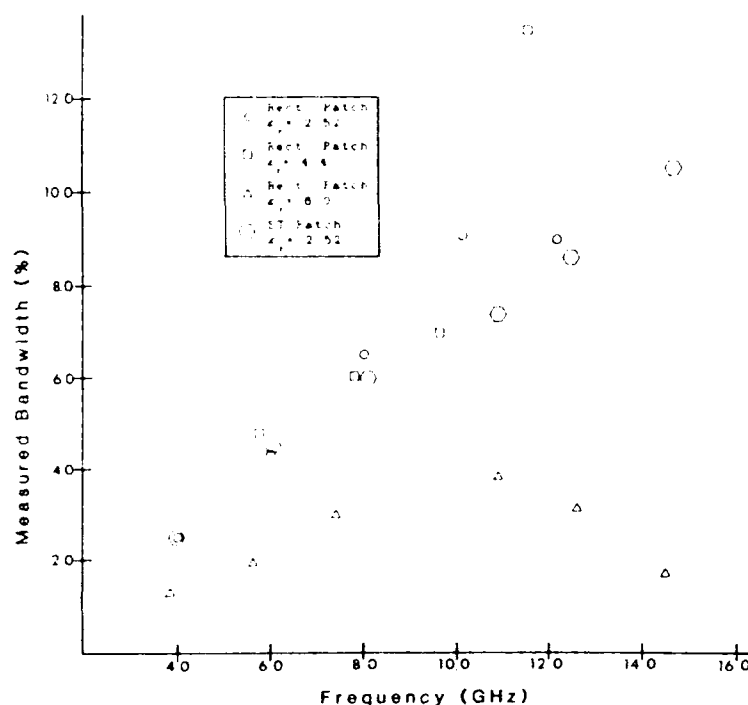


Figure 18. Measured 2:1 VSWR Bandwidth vs Resonant Frequency

#### 4.4 Stagger Tuned Patch Measurement Results

As mentioned earlier, seven stagger tuned patches were constructed on 1/16 in. PTFE ( $\epsilon_r = 2.52$ ,  $t = 0.0007$ ,  $\tan \delta = 0.0019$ ) with resonant frequencies between 4 and 16 GHz and tested. The model used for evaluating these patches was the transmission line model described in Section 3.2 and using Eqs. (1a) through (1c) for the main and stagger tuned section admittances and effective dielectric constants, respectively. Equation (8a) was used to compute the  $\Delta l$  values for slots 1 and 3 and Eq. (12a) was used to compute  $\Delta l_s$  for slot 2. Figure 19 shows the resonant frequency model error for all of the patches. The model error was low (less than 2 percent) up to about 12 GHz and progressively worsened for the higher frequencies. This trend is also reflected in the return loss values as seen in Appendix B. The bandwidth is given in Figure 18 and is about the same as for the standard rectangular patches on this material. But we expect this since there is only one mode resonating in both cases.

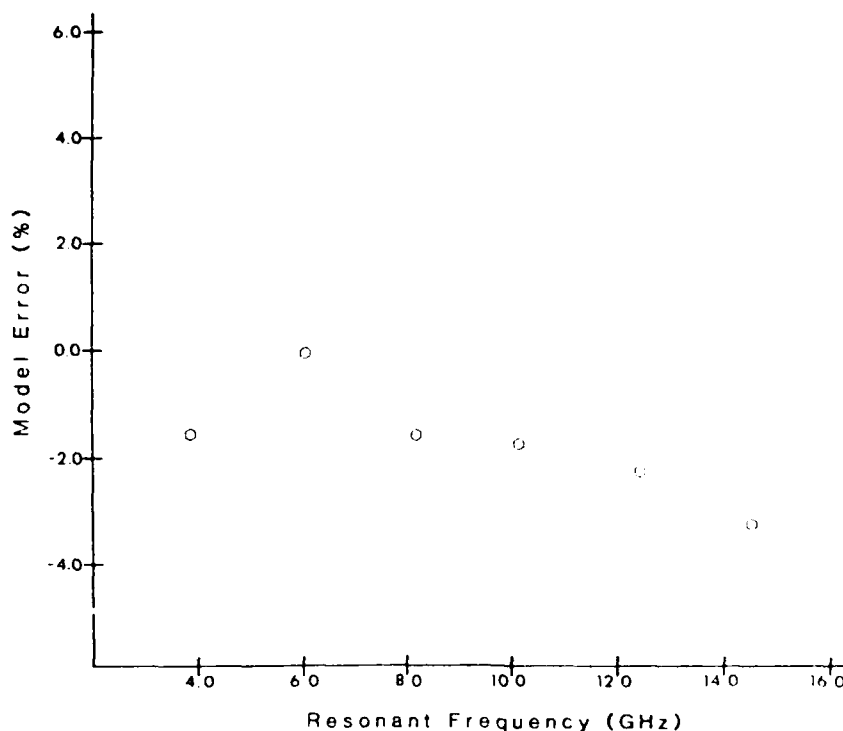


Figure 19. Stagger Tuned Patch Model Error vs Resonant Frequency

## 5. CONCLUSIONS AND RECOMMENDATIONS

In this report, many items pertaining to practical microstrip antenna design were investigated and discussed. A significant amount of data was also presented which the author hopes will be of use to practicing engineers in this field, including data on substrates, connectors, manufacturing tolerances, feed designs, surface waves, and dispersion. Two new versions of transmission line models were compared to the original version, measured results, and cavity model results for patches built on three different dielectric constant substrates. One version of the transmission line model achieved very good results; less than 0.7 percent average model error on the low  $\epsilon_r$  substrate compared to 3 percent error for the original model, but none of the transmission line models worked well on the high  $\epsilon_r$  substrates. The cavity model worked well on both the  $\epsilon_r = 2.52$  and 6.0 materials with less than 1.2 percent and 0.64 percent average error, respectively. Surprisingly, the cavity model even worked well for fairly thick ( $h \approx 0.1 \lambda_g$ ) substrates. The  $\epsilon_r = 4.4$  epoxy was deemed unacceptable for practical use due to its high loss tangent and varying material properties. However, it proved very useful as a case study for demonstrating the effects of high loss tangent substrates. The transmission line model also demonstrated the ability to model the stagger tuned patches with fairly good

accuracy (about 2 percent). Finally, there are many variations of both the transmission line model and cavity model left untried due to lack of time. I hope that someone else will extend this work.

## References

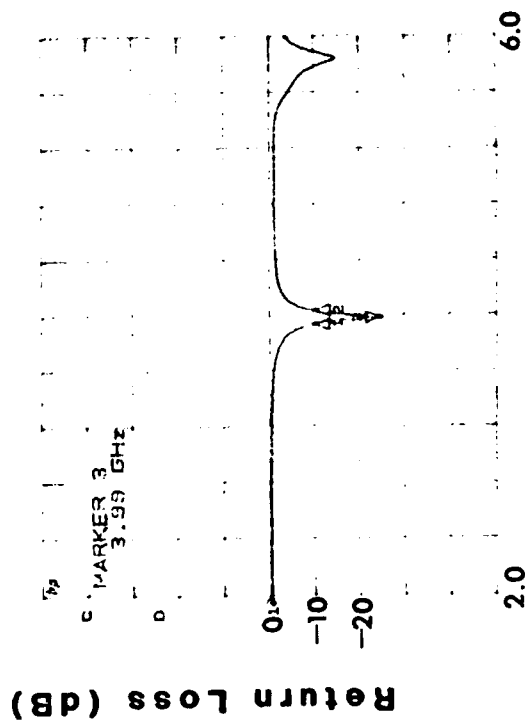
1. Munson, R.F. (1974) Conformal microstrip antennas and microstrip phased arrays. *IEEE Trans. Antennas and Propagation*, **AP-22**:74-78.
2. Carver, K.R. and Mink, J.W. (1981) Microstrip antenna technology, *IEEE Trans. Antennas and Propagation*, **AP-29**:25-37.
3. Bahl, J.I.J. and Garg, Ramesh (1977) Simple and Accurate Formulas for Microstrip with Finite Strip Thickness, *Proc. IEEE*, **65**:12161-1612.
4. Schneider, M.V. (1969) Microstrip Lines for Microwave Integrated Circuits, *Bell System Technical Journal*, pp. 1421-1444.
5. Hammerstadt, E.O. (1975) Equations for microstrip circuit design. *Proc. European Microwave Conference*, Hamburg, Germany, Sept. 1975, pp. 268-272.
6. Hammerstadt, E.O. and Jenson, O. (1980) Accurate models for microstrip computer aided design, *IEEE MTT-S Int. Microwave Symposium Digest*, pp. 407-409.
7. Harrington, R. (1961) *Time Harmonic Electromagnetic Fields*, McGraw-Hill, New York.
8. Pucis, H. and Van de Capelle, A. (1984) Accurate Transmission Line Model for the Rectangular Microstrip Antenna, *IEE Proc.*, **131**(Pt. H.):334-340.
9. Gogoi, A. and Gupta, K.C. (1982) Weiner-Hopf Computation of Edge Admittances for Microstrip Patch Radiators, *AEU*, **36**:464-467.
10. Silvester, P. and Benedek, P. (1972) Equivalent Capacitances of Microstrip Open Circuits, *IEEE Trans. On Microwave Theory and Techniques*, Vol. **MTT-20** (No. 8):511-516.
11. Hoffman, R.K. (1987) *Handbook of Microwave Integrated Circuits*, Artech House.

12. Kirschning, M., Jansen, R.H., and Koster, N.H.L. (1981) Accurate Model for Open End Effect of Microstrip Lines, *Electronics Letters*, 17 (No. 3):123-124.
13. Gupta, K.C., Garg, R., and Chadha, R. (1981) *Computer Aided Design of Microwave Circuits*, Artech House.
14. Pozar, D.M. (1987) Trimming Stubs for Microstrip Feed Networks and Patch Antennas, *IEEE Antennas and Propagation Society Newsletter*, Dec. 1987.
15. Carver, K.R. (1979) Practical Analytical Techniques for the Microstrip Antenna, *Proc. Workshop on Printed Circuit Antenna Tech.*, New Mexico State Univ., Oct 1979, pp. 7/1-20.
16. Chang, D.C. and Kuester, E.F. (1979) Resonance Characteristics of a Rectangular Microstrip Antenna, *Proc. Workshop on Printed Circuit Antenna Tech.*, New Mexico State University, Oct 1979, pp. 28/1-18.
17. Mittra, R. and Lee, S.W. (1971) *Analytical Technique in the Theory of Guided Waves*, Macmillan Co., New York.
18. Knuth, E.J. and Major, R.W. (1989) *Broadband Microstrip Components for EHF Steerable Antenna Arrays*, Naval Ocean Systems Center Technical Report 1278.
19. McGrath, D.T. and Fitzgerald, M.R. (1987) *Investigation of Surface Wave Blindness in Microstrip Phased Array Antennas*, RADC In-House Report RADC-TR-87-39, ADA189326.
20. Woernbke, J.D. (1982) Soft substrates conquer hard designs, *Microwaves*, January 1982.
21. Bahl, I.J. and Bhartia, P. (1980) *Microstrip Antennas*, Artech House.
22. Gupta, K.C. and Benalla, A. (1988) *Microstrip Antenna Design*, Artech House.
23. James, J.R., Hall, P.S., and Wood, C. (1981) *Microstrip Antenna Theory and Design*, Peter Peregrinus Ltd.

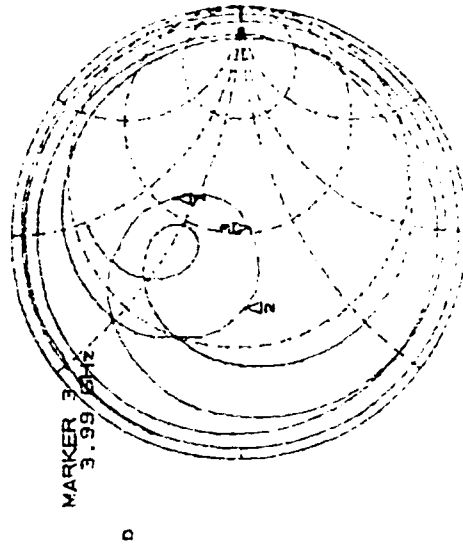
## **Appendix A**

### **Rectangular Patch Measurements**

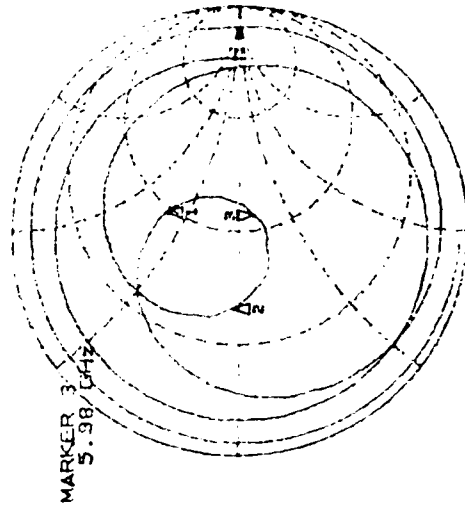
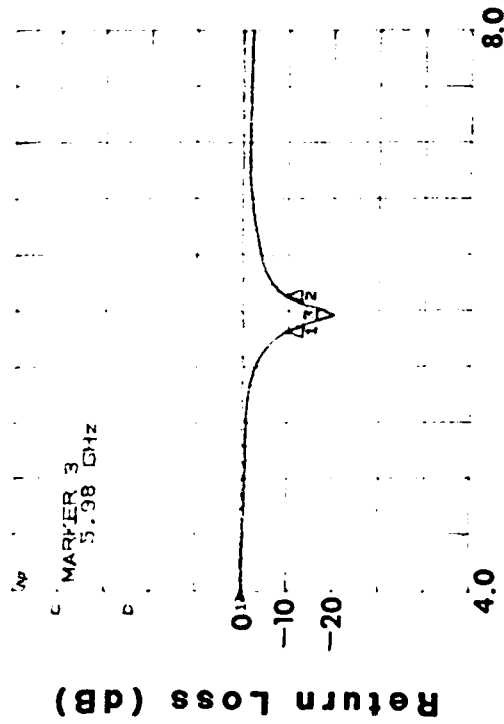




Frequency (GHz)



4.0 GHz Rectangular Patch  
 $\epsilon_r = 2.52$ ,  $h = 0.0625$ ,  $t = 0.0007$   
 Marker 1 = 3.94 GHz  
 Marker 2 = 4.04 GHz  
 Marker 3 = 3.99 GHz

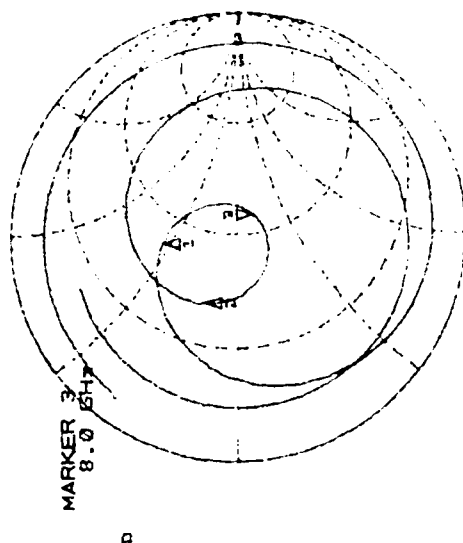
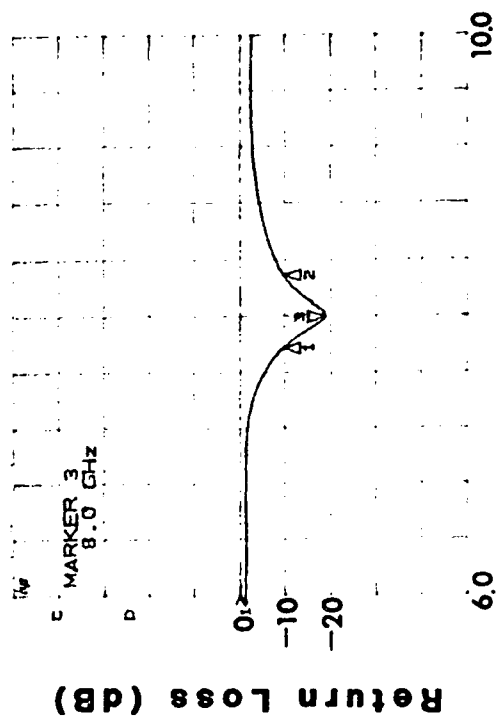


6.0 GHz Rectangular Patch  
 $\epsilon_r = 2.52$ ,  $h = 0.0625$ ,  $t = 0.0007$

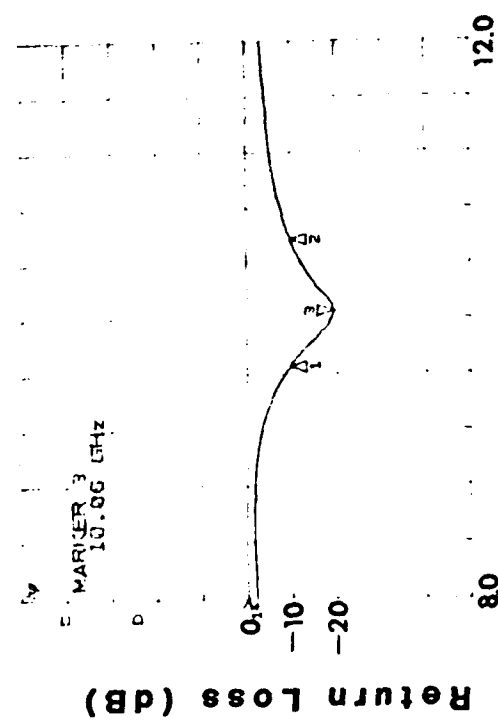
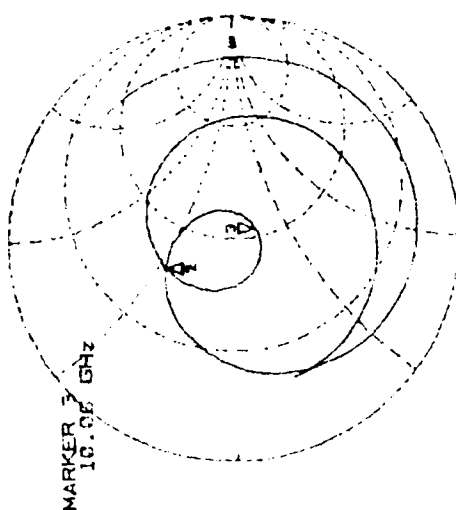
Marker 1 = 5.86 GHz

Marker 2 = 6.12 GHz

Marker 3 = 5.98 GHz

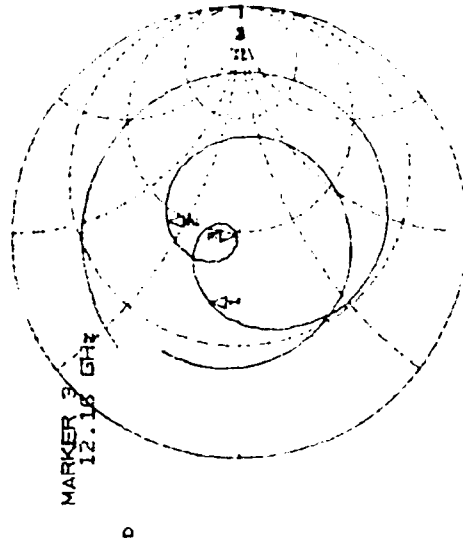
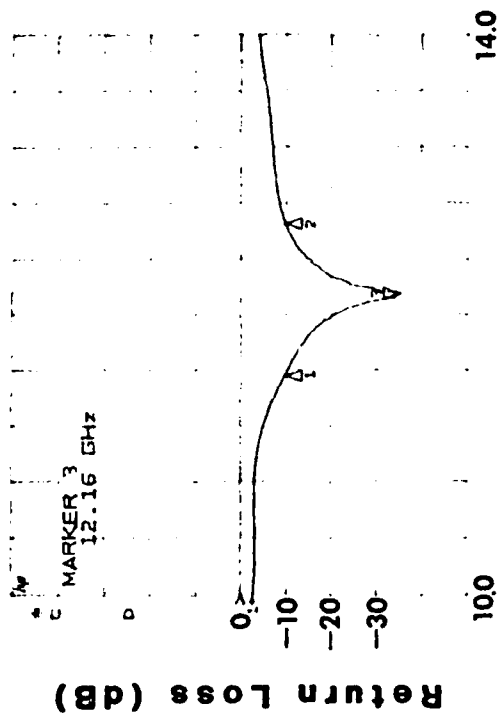


8.0 GHz Rectangular Patch  
 $\epsilon_r = 2.52$ ,  $h = 0.0625$ ,  $t = 0.0007$   
 Marker 1 = 7.78 GHz  
 Marker 2 = 8.30 GHz  
 Marker 3 = 8.00 GHz

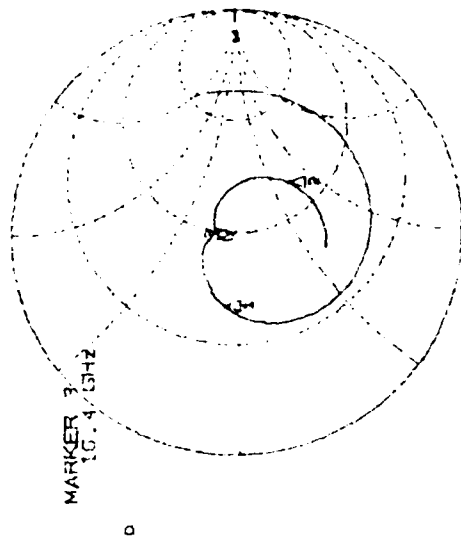
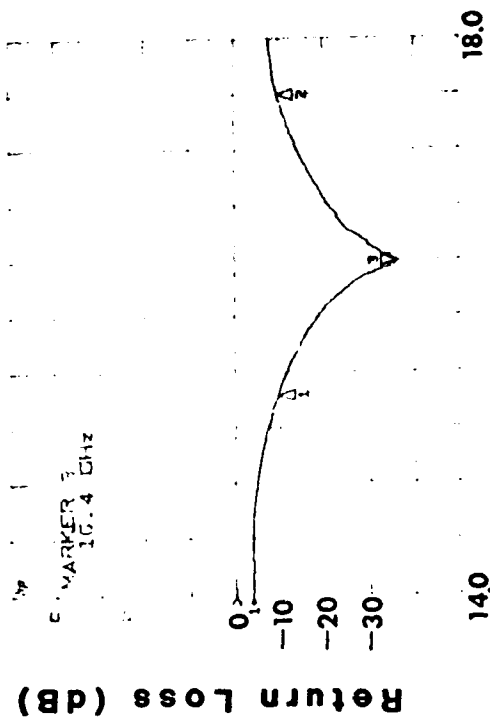


Frequency (GHz)

10.0 GHz Rectangular Patch  
 $\epsilon_r = 2.52$ ,  $h = 0.0625$ ,  $t = 0.0007$   
 Marker 1 = 9.66 GHz  
 Marker 2 = 10.58 GHz  
 Marker 3 = 10.06 GHz



12.0 GHz Rectangular Patch  
 $\epsilon_r = 2.52$ ,  $h = 0.0625$ ,  $t = 0.0007$   
 Marker 1  $\approx 11.56$  GHz  
 Marker 2  $\approx 12.66$  GHz  
 Marker 3  $\approx 12.16$  GHz



### Frequency (GHz)

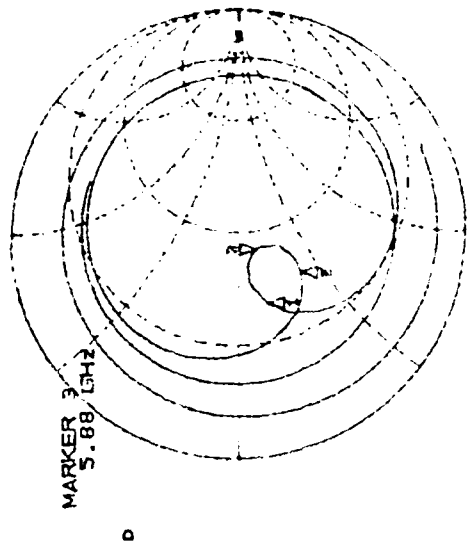
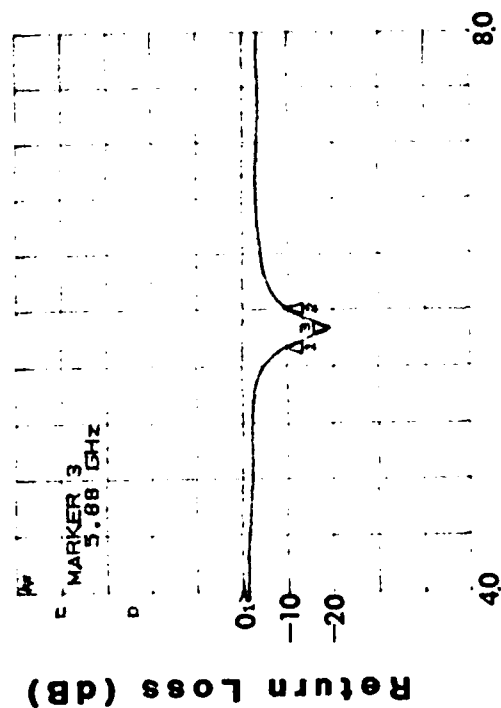
16.0 GHz Rectangular Patch

$\epsilon_r = 2.52$ ,  $h = 0.0625$ ,  $t = 0.0007$

Marker 1 = 15.44 GHz

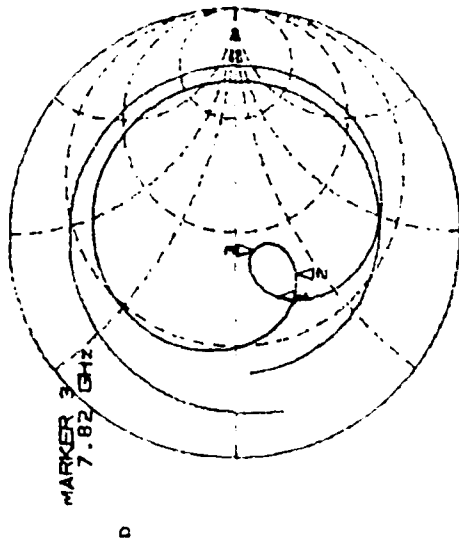
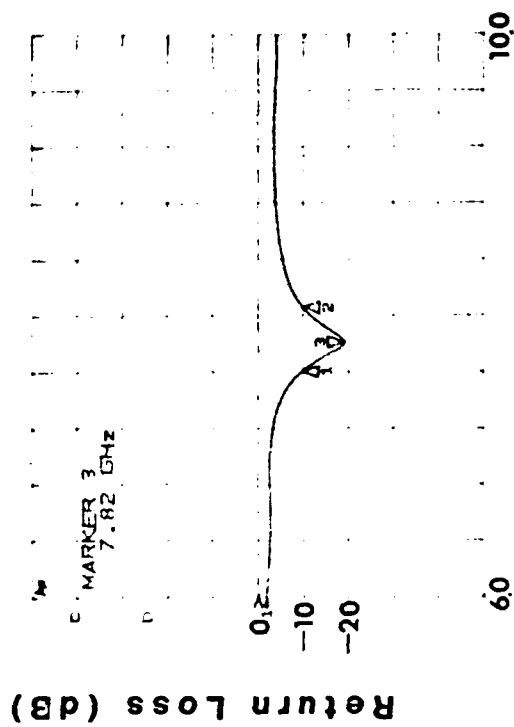
Marker 2 = 17.60 GHz

Marker 3 = 16.40 GHz



Frequency (GHz)

6.0 GHz Rectangular Patch  
 $\epsilon_r = 4.4$ ,  $h = 0.0625$ ,  $t = 0.0014$   
 Marker 1 = 5.74 GHz  
 Marker 2 = 6.02 GHz  
 Marker 3 = 5.88 GHz



### Frequency (GHz)

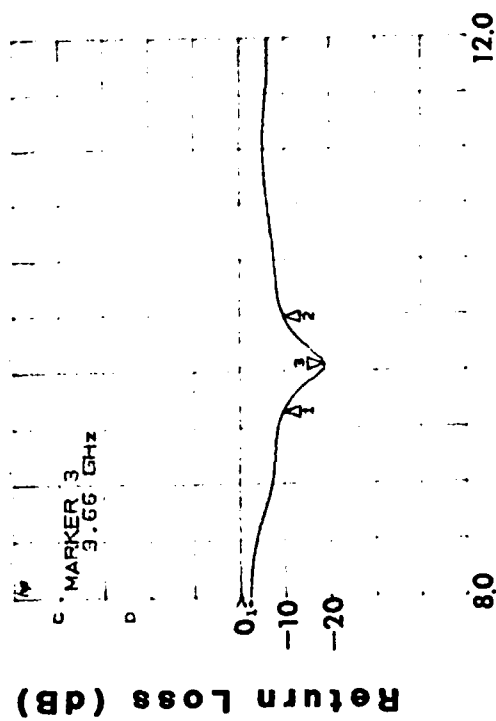
8.0 GHz Rectangular Patch  
 $\epsilon_r = 4.4$ ,  $h = 0.0625$ ,  $t = 0.0014$

Marker 1 = 7.60 GHz

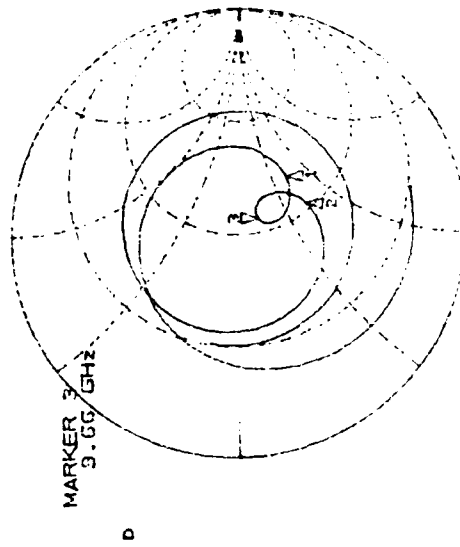
Marker 2 = 8.07 GHz

Marker 3 = 7.82 GHz

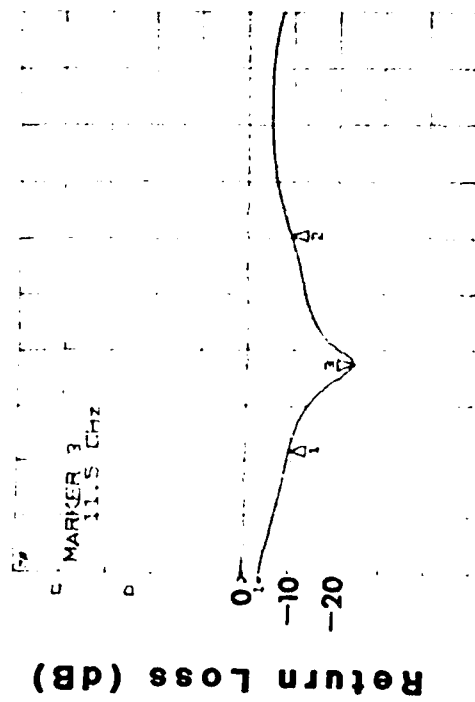




Frequency (GHz)



10.0 GHz Rectangular Patch  
 $\epsilon_r = 4.4$ ,  $h = 0.0625$ ,  $t = 0.0014$   
 Marker 1 = 9.32 GHz  
 Marker 2 = 10.00 GHz  
 Marker 3 = 9.66 GHz



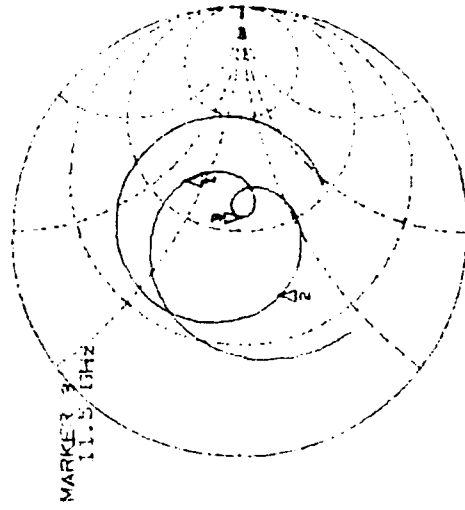
**Frequency (GHz)**

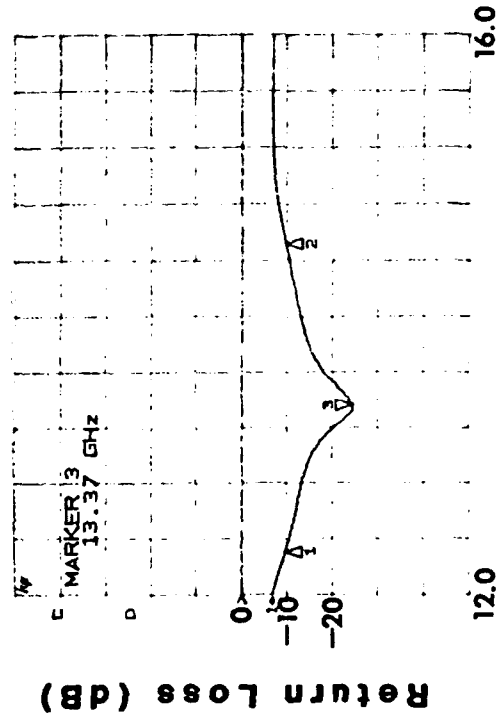
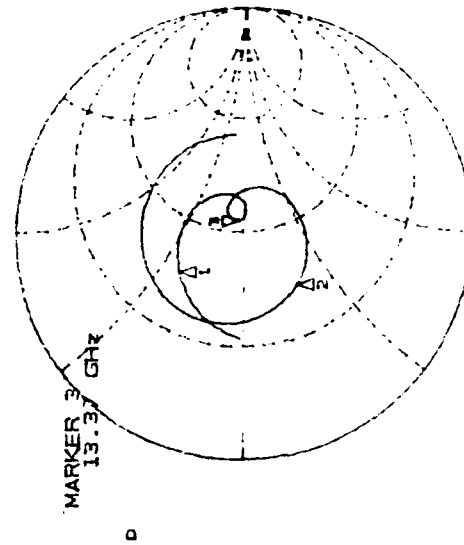
12.0 GHz Rectangular Patch  
 $\epsilon_r = 4.4$ ,  $h = 0.0625$ ,  $t = 0.0014$

Marker 1 = 10.88 GHz

Marker 2 = 12.43 GHz

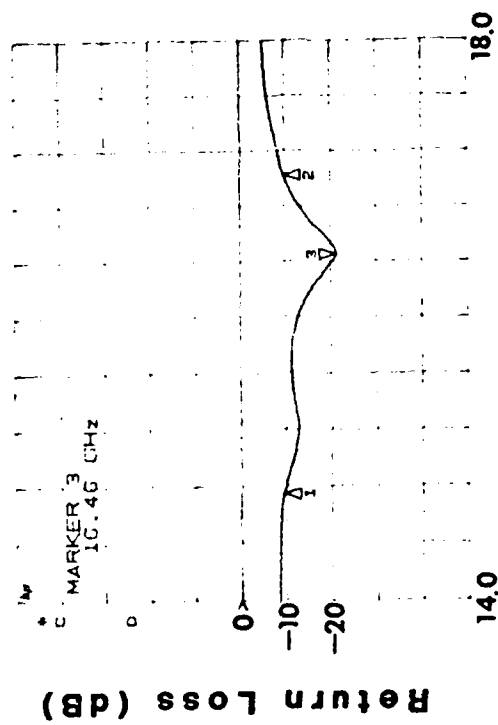
Marker 3 = 11.50 GHz





### Frequency (GHz)

14.0 GHz Rectangular Patch  
 $\epsilon_r = 4.4$ ,  $h = 0.0625$ ,  $t = 0.0014$   
 Marker 1 = 12.30 GHz  
 Marker 2 = 14.52 GHz  
 Marker 3 = 13.37 GHz



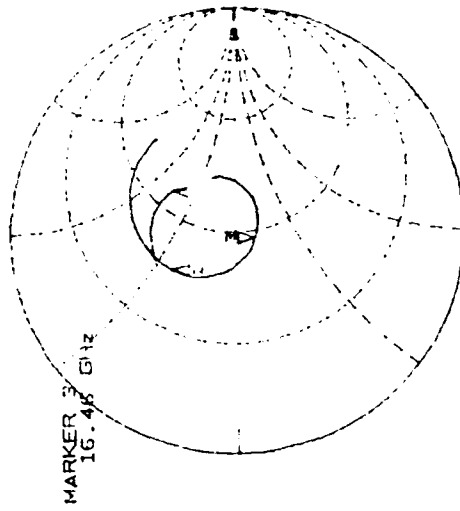
### Return Loss (dB)

16.0 GHz Rectangular Patch  
 $\epsilon_r = 4.4$ ,  $h = 0.0625$ ,  $t = 0.0014$

Marker 1 = 14.75 GHz

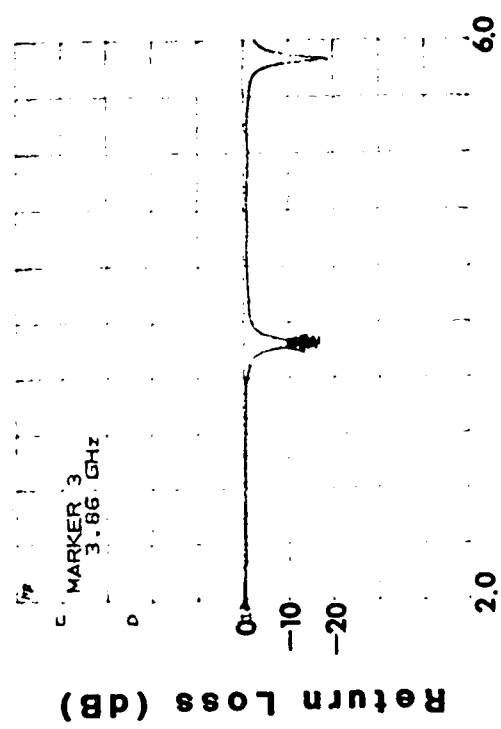
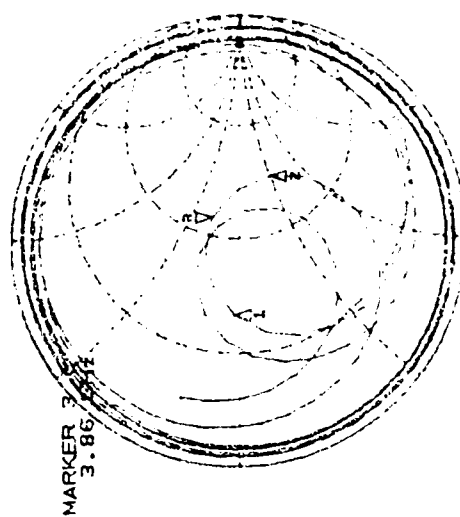
Marker 2 = 17.03 GHz

Marker 3 = 16.46 GHz



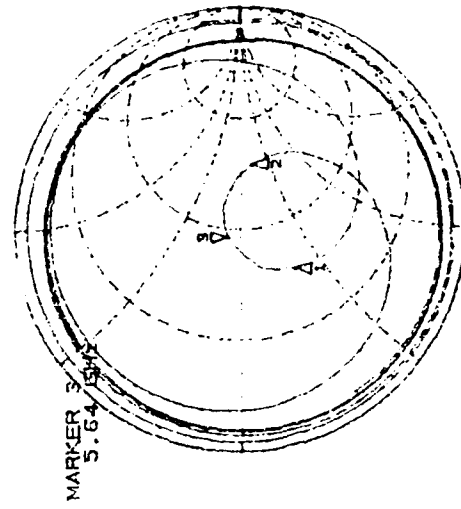
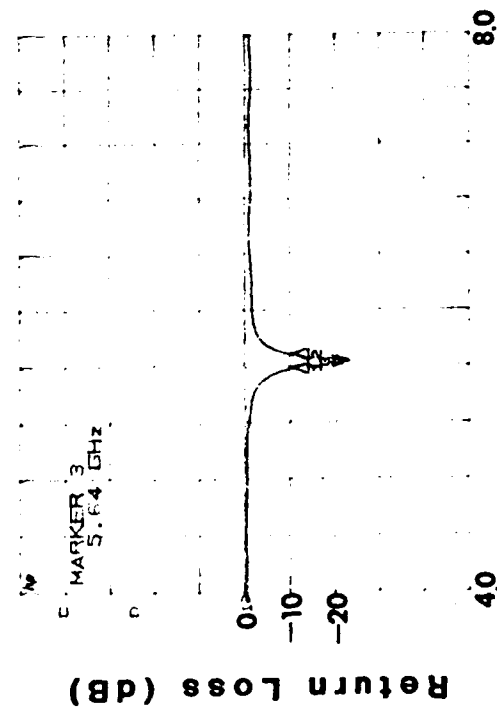
MARKER 3  
16.46 GHz

D



### Frequency (GHz)

4.0 GHz Rectangular Patch  
 $\epsilon_r = 6.00$ ,  $h = 0.050$ ,  $t = 0.0007$   
 Marker 1 = 3.83 GHz  
 Marker 2 = 3.88 GHz  
 Marker 3 = 3.86 GHz



### Frequency (GHz)

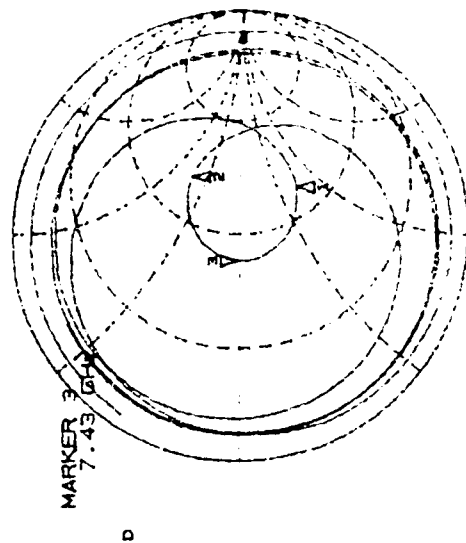
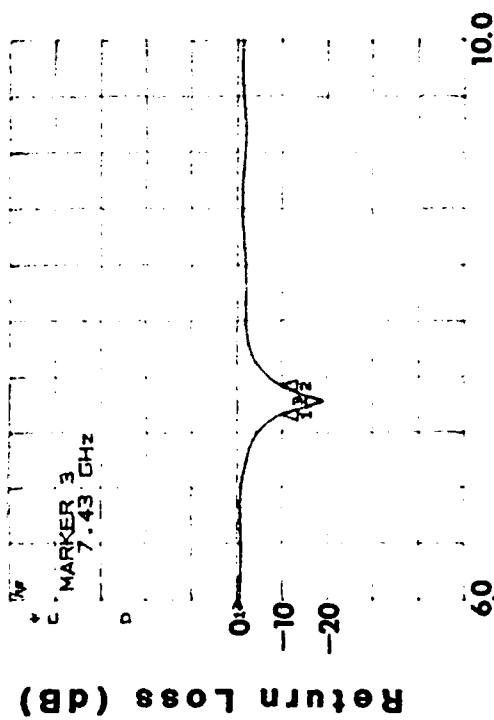
6.0 GHz Rectangular Patch

$\epsilon_r = 6.00$ ,  $h = 0.050$ ,  $t = 0.0007$

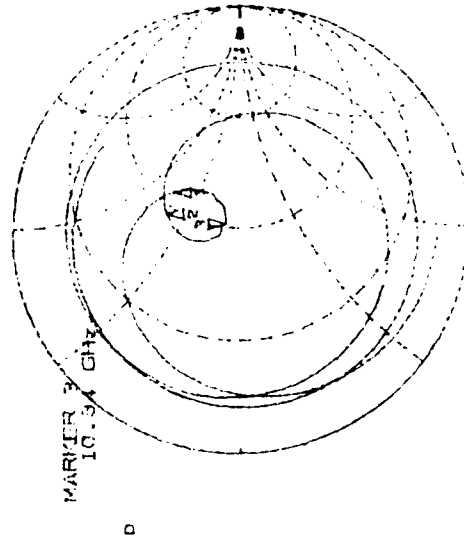
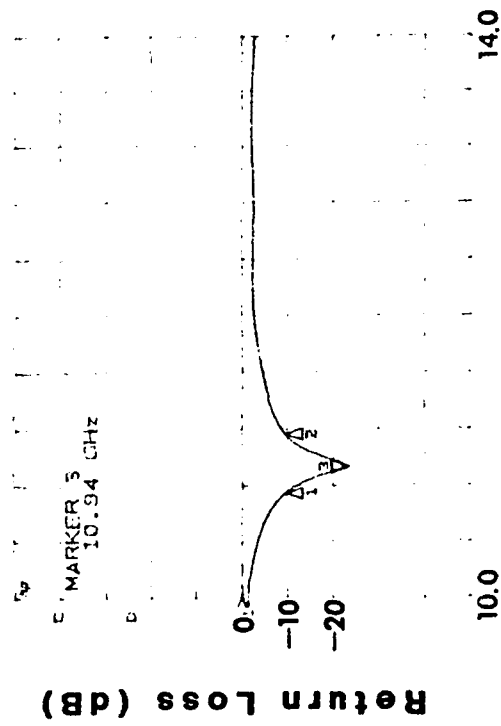
Marker 1 = 5.58 GHz

Marker 2 = 5.69 GHz

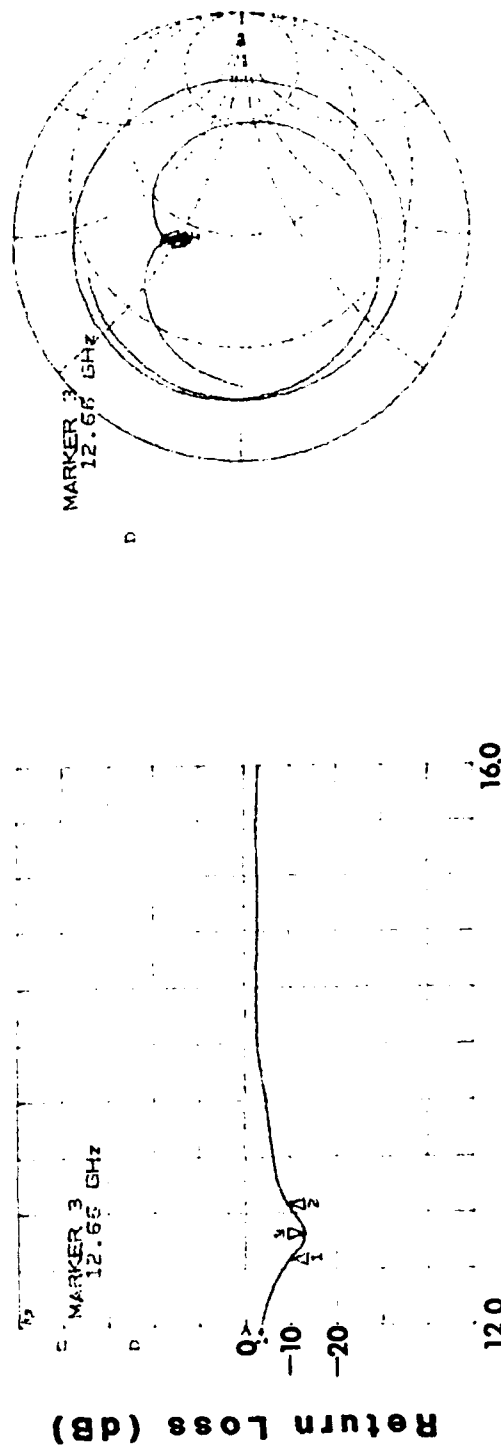
Marker 3 = 5.64 GHz



8.0 GHz Rectangular Patch  
 $\epsilon_r = 6.00$ ,  $h = 0.050$ ,  $t = 0.0007$   
 Marker 1 = 7.32 GHz  
 Marker 2 = 7.54 GHz  
 Marker 3 = 7.43 GHz





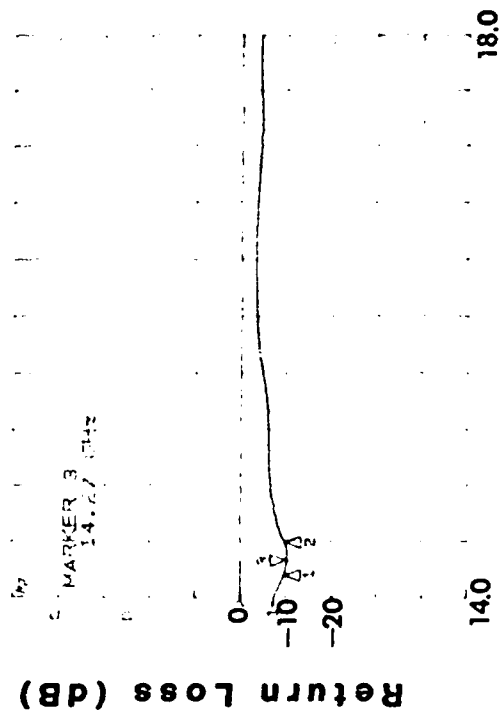


14.0 GHz Rectangular Patch  
 $\epsilon_r = 6.00$ ,  $h = 0.050$ ,  $t = 0.0007$

Marker 1 = 12.48 GHz

Marker 2 = 12.87 GHz

Marker 3 = 12.66 GHz



### Frequency (GHz)

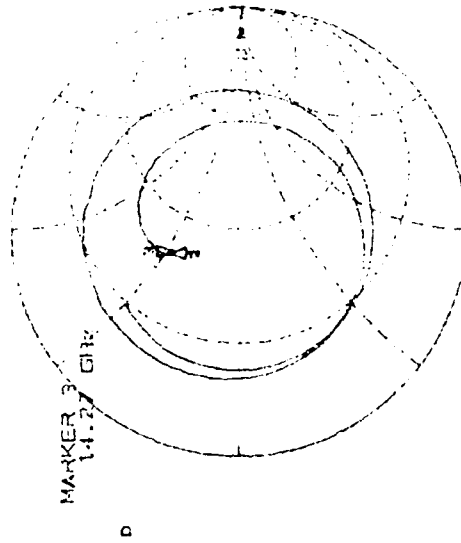
16.0 GHz Rectangular Patch

$\epsilon_r = 6.00$ ,  $h = 0.050$ ,  $t = 0.0007$

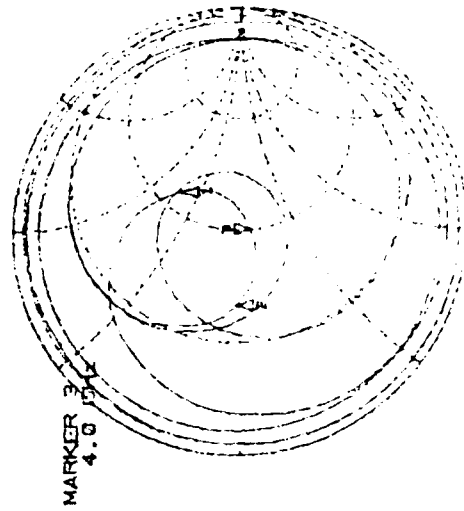
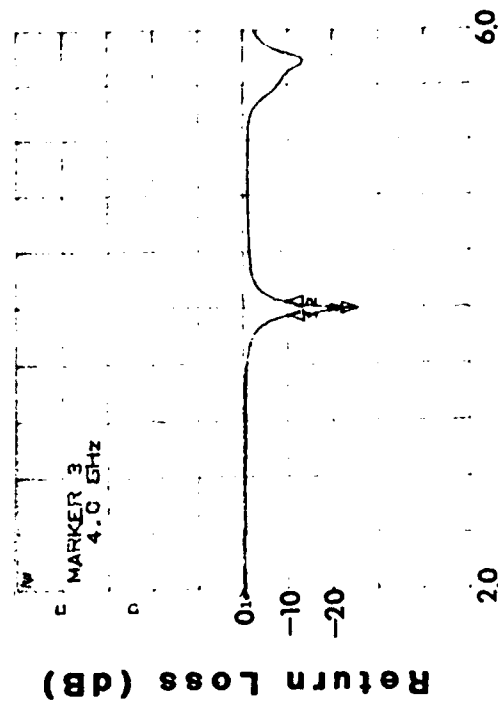
Marker 1 = 14.16 GHz

Marker 2 = 14.40 GHz

Marker 3 = 14.27 GHz



**Appendix B**  
**Stagger Tuned Patch Measurements**

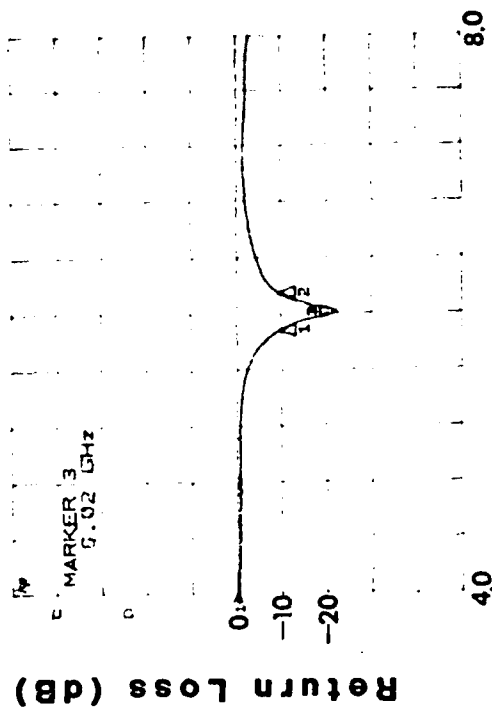


4.0 GHz Stagger Tuned Patch  
 $\epsilon_r = 2.52$ ,  $h = 0.0625$ ,  $t = 0.0007$

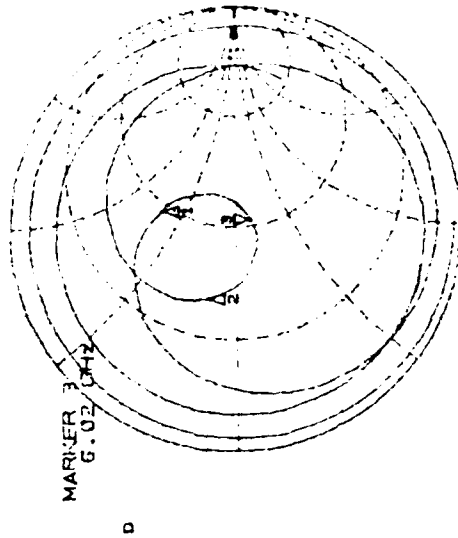
Marker 1 = 3.94 GHz

Marker 2 = 4.04 GHz

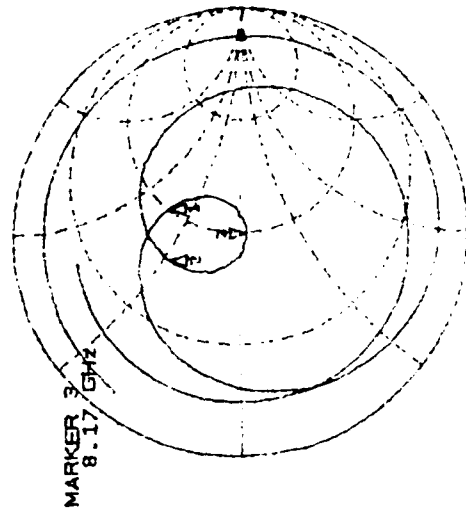
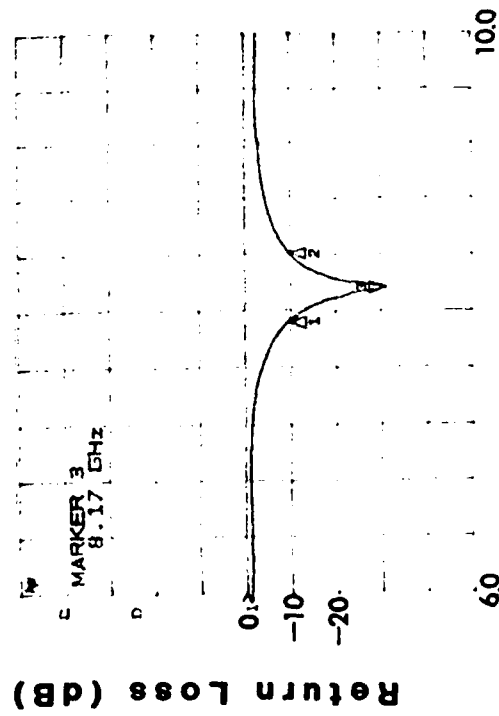
Marker 3 = 4.00 GHz



### Frequency (GHz)



6.0 GHz Stagger Tuned Patch  
 $\epsilon_r = 2.52$ ,  $h = 0.0625$ ,  $t = 0.0007$   
 Marker 1 = 5.89 GHz  
 Marker 2 = 6.16 GHz  
 Marker 3 = 6.02 GHz

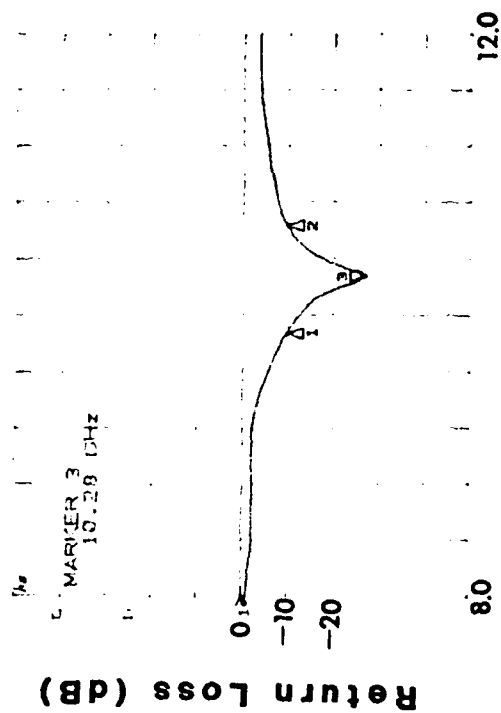


8.0 GHz Stagger Tuned Patch  
 $\epsilon_r = 2.52$ ,  $h = 0.0625$ ,  $t = 0.0007$

Marker 1 = 7.93 GHz

Marker 2 = 8.42 GHz

Marker 3 = 8.17 GHz



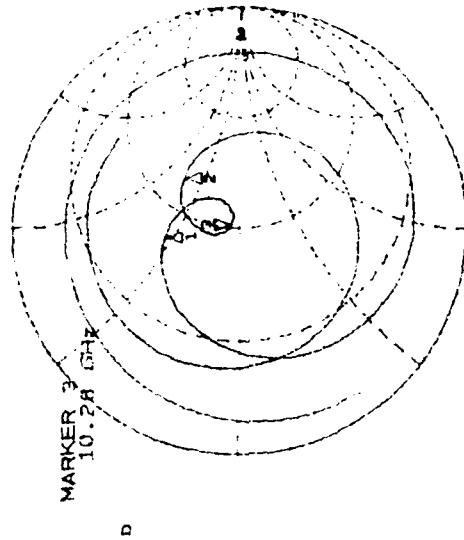
### Frequency (GHz)

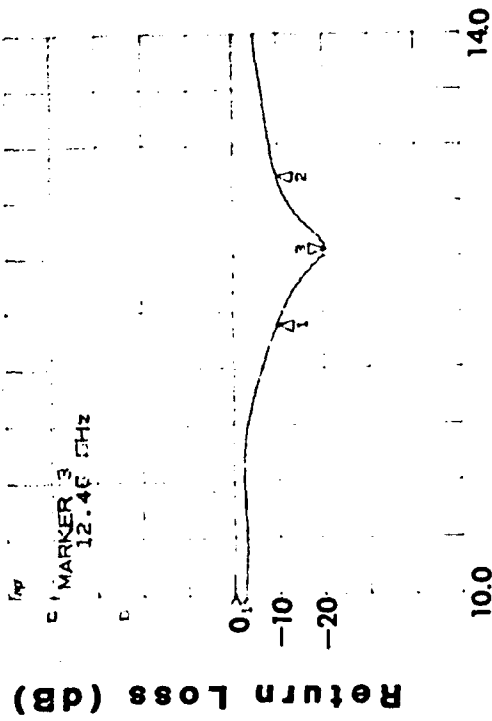
10.0 GHz Stagger Tuned Patch  
 $\epsilon_r = 2.52$ ,  $h = 0.0625$ ,  $t = 0.0007$

Marker 1 = 9.88 GHz

Marker 2 = 10.64 GHz

Marker 3 = 10.28 GHz





### Frequency (GHz)

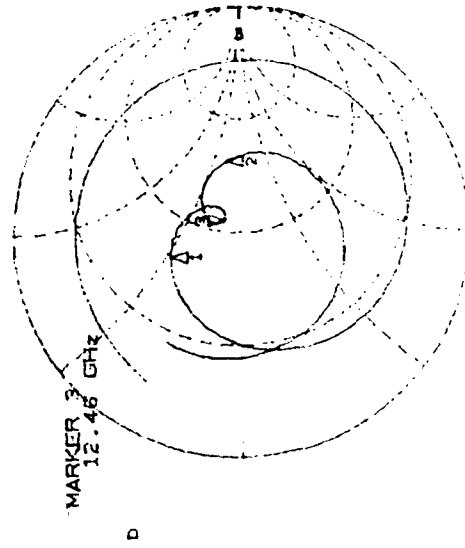
12.0 GHz Stagger Tuned Patch

$\epsilon_r = 2.52$ ,  $h = 0.0625$ ,  $t = 0.0007$

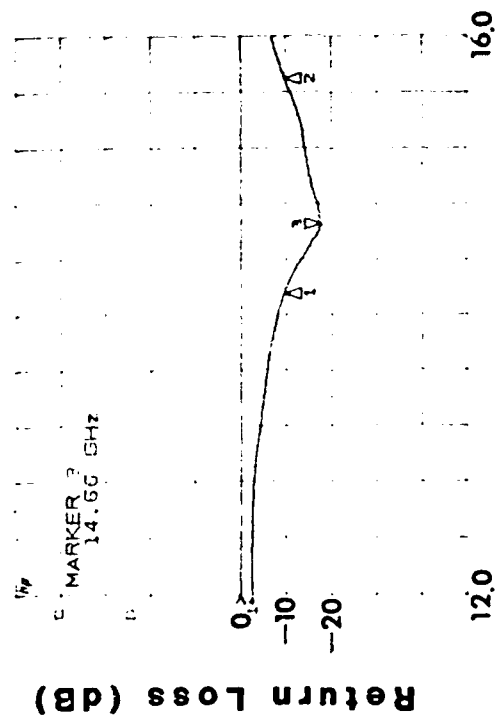
Marker 1 = 11.91 GHz

Marker 2 = 12.98 GHz

Marker 3 = 12.46 GHz







### Frequency (GHz)

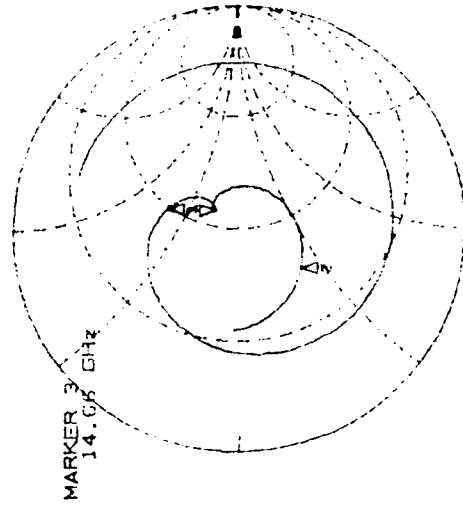
14.0 GHz Stagger Tuned Patch

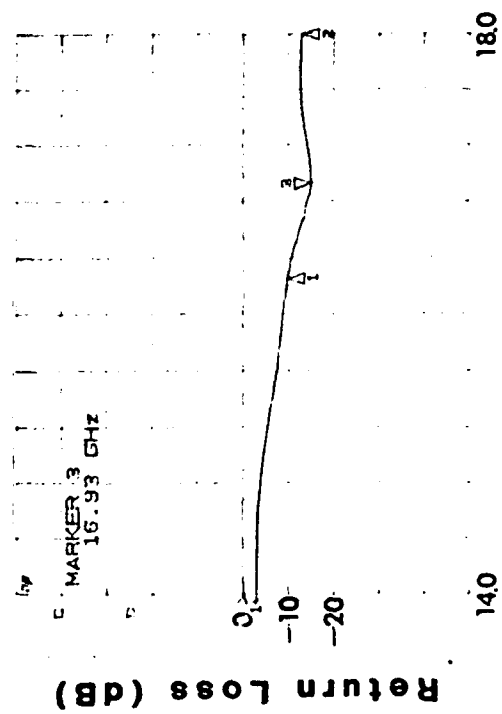
$\epsilon_r = 2.52$ ,  $h = 0.0625$ ,  $t = 0.0007$

Marker 1 = 14.16 GHz

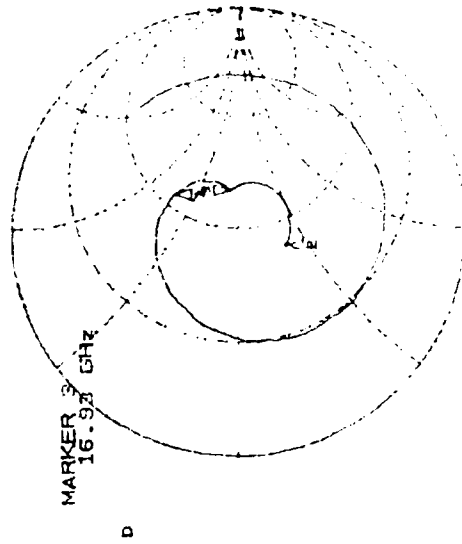
Marker 2 = 15.70 GHz

Marker 3 = 14.66 GHz





### Frequency (GHz)



16.0 GHz Stagger Tuned Patch  
 $\epsilon_r = 2.52$ ,  $h = 0.0625$ ,  $t = 0.0007$

Marker 1 = 16.26 GHz

Marker 2 = 18.00 GHz

Marker 3 = 16.93 GHz

**MISSION  
OF  
ROME LABORATORY**

*Rome Laboratory plans and executes an interdisciplinary program in research, development, test, and technology transition in support of Air Force Command, Control, Communications and Intelligence (C<sup>3</sup>I) activities for all Air Force platforms. It also executes selected acquisition programs in several areas of expertise. Technical and engineering support within areas of competence is provided to ESD Program Offices (POs) and other ESD elements to perform effective acquisition of C<sup>3</sup>I systems. In addition, Rome Laboratory's technology supports other AFSC Product Divisions, the Air Force user community, and other DOD and non-DOD agencies. Rome Laboratory maintains technical competence and research programs in areas including, but not limited to, communications, command and control, battle management, intelligence information processing, computational sciences and software producibility, wide area surveillance/sensors, signal processing, solid state sciences, photonics, electromagnetic technology, superconductivity, and electronic reliability/maintainability and testability.*